LASER INTERFEROMETER GRAVITATIONAL WAVE OBSERVATORY
- LIGO -
CALIFORNIA INSTITUTE OF TECHNOLOGY
MASSACHUSETTS INSTITUTE OF TECHNOLOGY

Technical Note	**LIGO-T1000298–T**	**2010/06/02**

Advanced LIGO Length Sensing and Control Final Design

Rich Abbott, Rana Adhikari, Stefan Ballmer, Lisa Barsotti, Matt Evans, Peter Fritschel, Valera Frolov, Guido Mueller, Bram Slagmolen, Sam Waldman

Distribution of this document:

ISC FDR Committee

This is an internal working note of the LIGO project

California Institute of Technology
LIGO Project, MS 18-34
Pasadena, CA 91125
Phone (626) 395-2129
Fax (626) 304-9834
E-mail: info@ligo.caltech.edu

Massachusetts Institute of Technology
LIGO Project, Room NW22-295
Cambridge, MA 02139
Phone (617) 253-4824
Fax (617) 253-7014
E-mail: info@ligo.mit.edu

LIGO Hanford Observatory
Route 10, Mile Marker 2
Richland, WA 99352
Phone (509) 372-8106
Fax (509) 372-8137
E-mail: info@ligo.caltech.edu

LIGO Livingston Observatory
19100 LIGO Lane
Livingston, LA 70754
Phone (225) 686-3100
Fax (225) 686-7189
E-mail: info@ligo.caltech.edu

http://www.ligo.caltech.edu/

Abstract

We present the final design and supporting analysis for the Advanced LIGO Detector Length Sensing and Control subsystem.

1 LSC subsystem description

1.1 Subsystem Context

The Length Sensing and Control (LSC) Subsystem is responsible for maintaining optical resonance in the Dual-Recycled Fabry-Perot Michelson (DRFPM) interferometer. It is also responsible for providing the Gravitational Wave (GW) readout signal. This includes photodetectors, demodulation electronics, A/D converter and the computer hard and software. The design of the DC-readout and Output Mode Cleaner (OMC) is described in a separate document ([**?**]). Also, the lock acquisition (LA) procedure is presented in a separate document ([1]). The LSC interfaces with the Suspension (SUS) Subsystem for the actuation on the optics, and with the Pre-Stabilized Laser (PSL) for actuation on the laser frequency. The design of the modulation and readout scheme is the shared responsibility of the LSC and ASC (alignment system). The modulation is implemented by Input Optics (IO), according to the requirements of the LSC and ASC.

1.2 States of operation

The Interferometer Sensing and Control (ISC) system has to bring the interferometer from the unlocked stage to a configuration appropriate for collecting science data. Much of this requirement is the responsability of the LSC subsystem, but it also involves other subsytems, in particular SUS, ASC and ALS (Arm Length Stabilization). This will involve the following states of operation:

1. Acquisition. In this state the length degrees-of-freedom go from being globally uncontrolled to globally controlled, and are brought to their operating points.
2. Transition. In this phase interferometer parameters such as control topology, input power and switchable filters are changed from the optimal values for lock acquisition to a configuration suitable for scientific data collecting.
3. Science mode. This is the traditional science mode as known from initial LIGO operation, during which science data is collected.

This document focuses on item 3, Science Mode. The lock acquisition process is described in [1]

1.3 Modes of operation

The LSC system is being designed to operate in different science modes, which have different levels of operational complexity and different sensitivity spectra. These modes, labeled 0, 1

and 2, are described in the Advanced LIGO Systems Final Design (SFD, [2]). Strain noise spectra for these modes are shown in Fig. 1 and operating parameters are given in Table 1.

mode 0 In this mode there is no signal recycling (SRM transmission of 100%), and modest input power (25 W). Since this configuration is so similar to the initial LIGO interferometer, we would expect to be able to get running in this mode fairly quickly, and start taking data with significantly better sensitivity than initial LIGO.

mode 1 In this mode there is broad-band signal recycling (i.e., no detuning of the signal recycling cavity). It is easier to get good error signals for all the degrees-of-freedom in this mode. This mode could run with different input powers (the spectra for two are shown below), presumably starting with low power. At high power, the sensitivity to NS-NS inspirals is almost as good as can be achieved by specifically tuning for them.

mode 2 This is the canonical optional mode at full power and the SRC tuned to optimize sensitivity to NS-NS inspirals. We have however fixed the SRM transmission at 20%, which is a bit higher than the optimum for NS-NS sensitivity, as a compromise with the broad-band case (the difference is less than 0.4%).

Mode	*NS-NS Range*	*BH-BH Range*	P_{in}	T_{SRM}	ϕ_{SRC}
0	150 Mpc	1.60 Gpc	25 W	100%	–
1a	145 Mpc	1.65 Gpc	25 W	20%	0 deg.
1b	190 Mpc	1.85 Gpc	125 W	20%	0 deg.
2	200 Mpc	1.65 Gpc	125 W	20%	16 deg.

Table 1: Parameters for the operational modes described above, and shown in Fig. 1. The homodyne detection phase is also optimized in each case, which in practice can be set via the Michelson dark fringe offset.

1.4 Interferometer Diagram

Refer to Fig. 2 for a block diagram of the interferometer, showing the LSC/ASC detection ports and the length degrees-of-freedom.

2 Modulation and Readout

2.1 Modulation

The laser light is phase modulated at two radio frequencies, $f_1 \approx 9$ MHz and $f_2 = 5f_1 \approx 45$ MHz. The two frequencies are phase-locked to avoid any beat from higher-order sidebands. We will use serial modulation in one crystal, i.e. we do not need a Mach-Zehnder interferometer (see appendix B). However a Mach-Zehnder could be retrofitted.

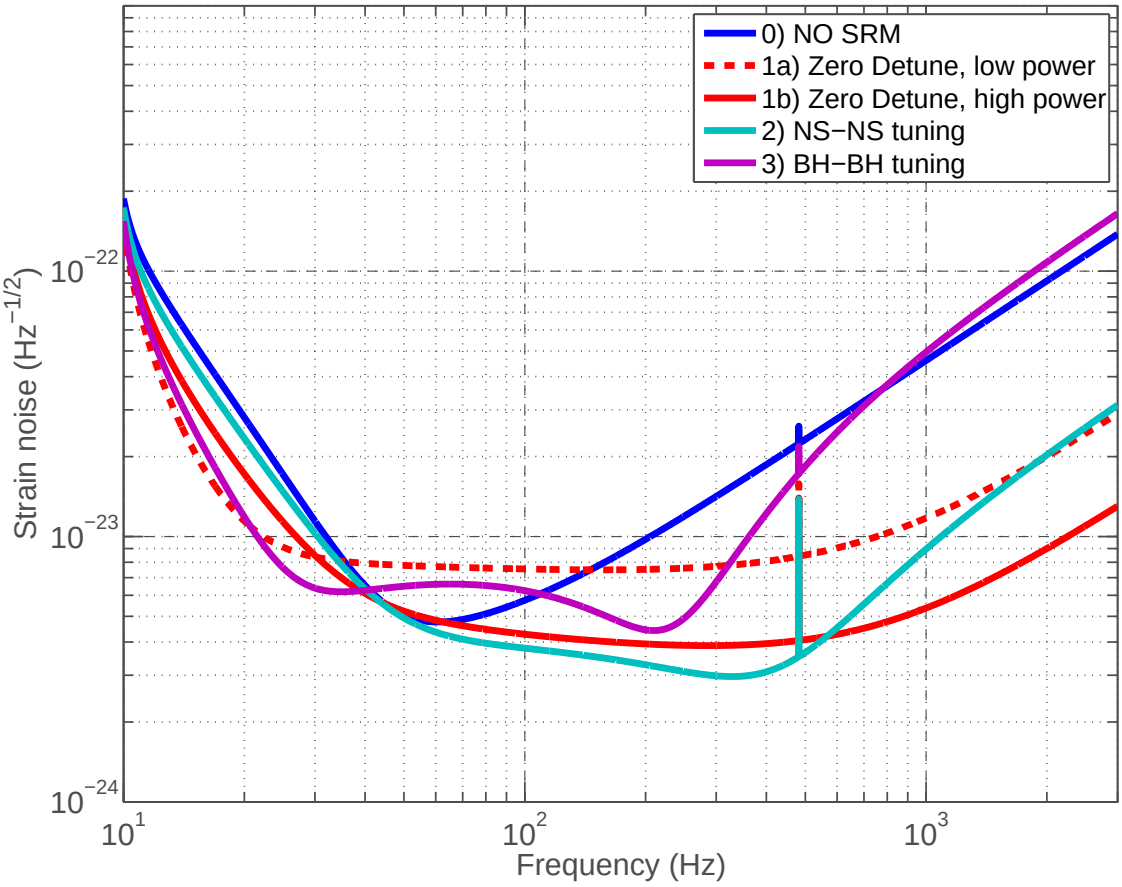

Figure 1: Proposed modes of operation for the Advanced LIGO interferometers. See text for description of the modes.

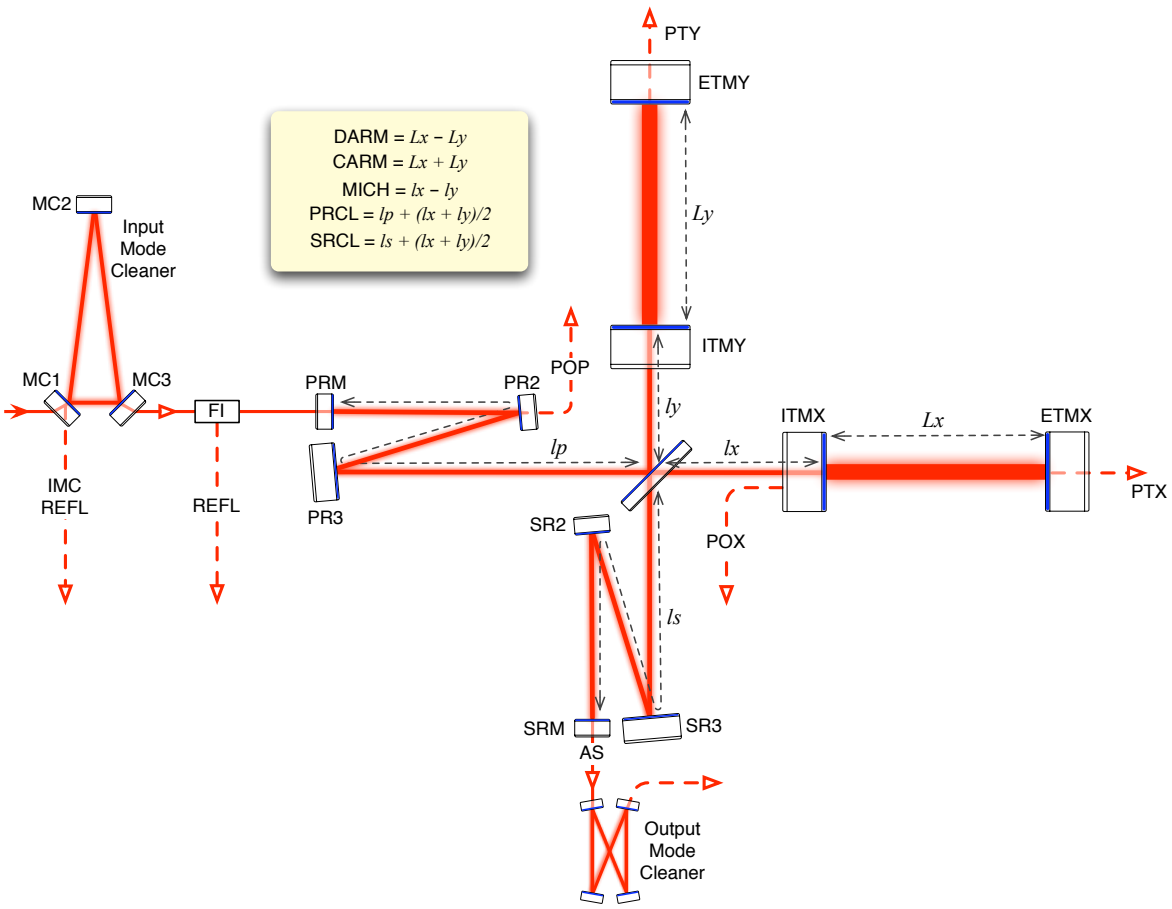

Figure 2: Interferometer diagram, showing LSC/ASC detection ports and length degrees-of-freedom. Port acronyms: REFL, reflection port; POP, power recycling cavity pick-off; POX, X arm pick-off; AS, anti-symmetric port; PTX/Y, transmitted power X/Y arm.

Quantity	*Non-Folded IFOs*	*Folded IFO*
Finesse	446	446
ITM transmission	0.014	0.014
PRM transmission	0.030	0.030
SRM transmission	0.200	0.200
Schnupp asymmetry	0.050	0.050
ETM radius of curvature	2245 m	2245 m
ITM radius of curvature	1934 m	1934 m
l_{PRC}	57.6557 m	60.4112 m
l_{SRC}	56.0084 m	62.1372 m
l_{IMC} (round trip)	32.9461 m	34.5207 m
l_{EX}	3994.50 m	3996.00 m
l_{EY}	3994.50 m	3996.00 m
Free Spectral Range (FSR)	37.526 kHz	37.512 kHz
Transverse mode spacing	32.453 kHz	32.462 kHz
Lower mod. frequency	9'099'471 Hz	8'684'428 Hz
Upper mod. frequency	45'497'355 Hz	43'422'140 Hz

Table 2: Basic interferometer parameters for both folded and non-folded case.

Additionally we want to avoid hitting arm resonances with a sideband, at least for the lowest order spatial arm modes. With test mass radii of curvature of 2245 m for the ETMs and 1934 m for the ITMs we get an arm cavity free spectral range of 37.526 kHz (37.512 kHz) the transverse mode spacing is 32.453 kHz (32.462 kHz). (Numbers in brackets are for the folded interfferometer.) Tables 3 and 4 show the minimal separations from arm cavity resonances for all sidebands. They use sideband frequencies of $f1 = 9'099'471$ Hz ($8'684'428$ Hz) and $f2 = 45'497'355$ Hz ($43'422'140$ MHz).

No higher order mode comes closer to resonance than about 940 Hz, and all modes closer than 2 kHz (roughly the upper end of the GW band of interest) are highlighted in red. Note that in initial LIGO audio sidebands of RF sidebands becoming resonant in the arms were responsible for a significant increase in the phase noise coupling [3].

Additionally, the frequencies and arm length were picked such that the $f1$ sideband is 500 Hz away from exactly anti-resonant in the arms, and thus the $f2$ sideband is 2500 Hz away from anti-resonant. This guarantees that the $f2$ sideband is far (about 16 kHz) away from resonance, which minimizes the arm-cavity phase shift the $f2$ sideband sees. This turns out to help the Michelson (MICH) shot noise sensitivity. The effect for Science mode was not dramatic - presumable because the $f2$ is resonant in the SRC. But it made a huge difference for No-SRM operation - a factor of 4 compared to the old parameters, see figure 3. Also note that the change to the sideband frequencies and cavity length in table 2 was made after most of the detailed Opickle modeling was done. The parameters used in the Opickle modeling are listed in table 6.

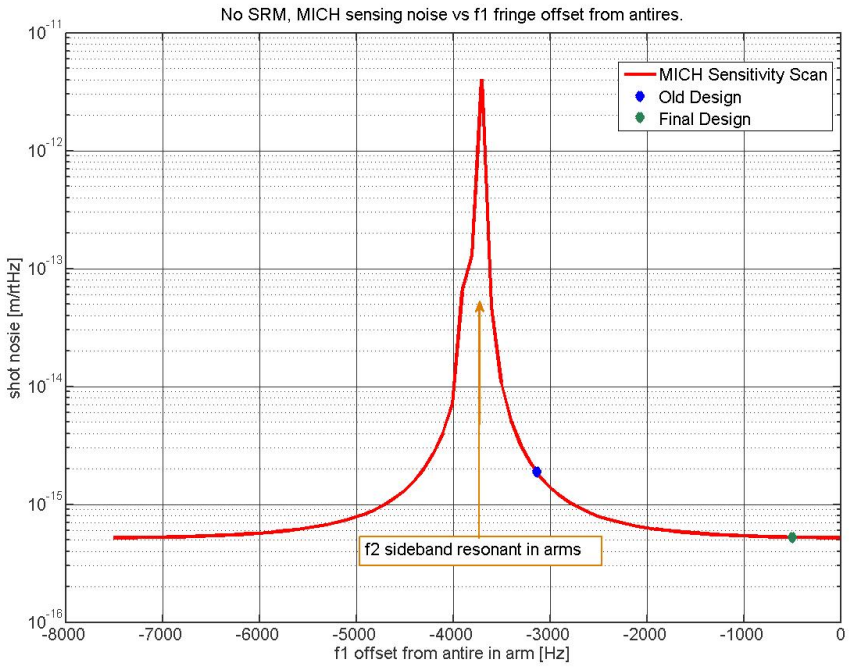

Figure 3: Michelson (MICH) shot noise sensitivity without signal recycling mirror (No SRM) plotted vs. the offset of $f1$ from exactly anti-resonant in the arms. $f2$ has 5 times the offset. The final design parameters (table 2) correspond to the green diamond, while the old design (table 6) is shown with the blue diamond.

Sideband offset from arm resonance, non-folded interferometer			
Upper low frequency sideband (f1=9.0995 MHz)			
# FSR offset	l+m	offset from resonance	offset from anti-resonance
242	0	**18.26** kHz	**500.3** Hz
242	1	14.19 kHz	
241	1		4572 Hz
241	2	9.119 kHz	
240	3	4.046 kHz	
239	4	**1.026** kHz	
238	5	6.098 kHz	
237	6	11.17 kHz	
Lower low frequency sideband (f1=9.0995 MHz)			
# FSR offset	l+m	offset from resonance	offset from anti-resonance
−242	0	**18.26** kHz	
−243	0		**500.3** Hz
−243	1	13.19 kHz	
−244	1		5573 Hz
−244	2	8.118 kHz	
−245	3	3.046 kHz	
−246	4	2.027 kHz	
−247	5	7.099 kHz	
−248	6	12.17 kHz	6592 Hz
Upper high frequency sideband (f2=45.4974 MHz)			
# FSR offset	l+m	offset from resonance	offset from anti-resonance
1212	0	**16.26** kHz	**2502** Hz
1212	1	16.19 kHz	
1211	1		2571 Hz
1211	2	11.12 kHz	
1210	3	6.048 kHz	
1209	4	**0.975** kHz	
1208	5	4.097 kHz	
1207	6	9.169 kHz	
Lower high frequency sideband (f2=45.4974 MHz)			
# FSR offset	l+m	offset from resonance	offset from anti-resonance
−1212	0	**16.26** kHz	
−1213	0		**2502** Hz
−1213	1	11.19 kHz	
−1214	2	6.117 kHz	
−1215	3	**1.044** kHz	
−1216	4	4.028 kHz	
−1217	5	9.1 kHz	
−1218	6	14.17 kHz	4590 Hz

Table 3: Table showing the closest sideband resonances in the arm cavities up to spatial modes with $l + m = 6$. Separation from exact anti-resonance is shown in column 4 if it is closer than 7 kHz. All offsets less than 2 kHz are highlighted in red, and the offsets of the $l + m = 0$ mode are highlighted in blue. This table is for the non-folded interferometers.

Sideband offset from arm resonance, folded interferometer

Upper low frequency sideband (f1=8.6844 MHz)			
# FSR offset	l+m	offset from resonance	offset from anti-resonance
232	0	**18.26** kHz	
231	0		**499.8** Hz
231	1	13.21 kHz	
230	1		5549 Hz
230	2	8.157 kHz	
229	3	3.108 kHz	
228	4	**1.942** kHz	
227	5	6.991 kHz	
226	6	12.04 kHz	6715 Hz
Lower low frequency sideband (f1=8.6844 MHz)			
# FSR offset	l+m	offset from resonance	offset from anti-resonance
−232	0	**18.26** kHz	**499.8** Hz
−232	1	14.21 kHz	
−233	1		4550 Hz
−233	2	9.157 kHz	
−234	3	4.107 kHz	
−235	4	**0.942** kHz	
−236	5	5.991 kHz	
−237	6	11.04 kHz	
Upper high frequency sideband (f2=43.4221 MHz)			
# FSR offset	l+m	offset from resonance	offset from anti-resonance
1158	0	**16.26** kHz	
1157	0		**2499** Hz
1157	1	11.21 kHz	
1156	2	6.158 kHz	
1155	3	**1.108** kHz	
1154	4	3.941 kHz	
1153	5	8.99 kHz	
1152	6	14.04 kHz	4716 Hz
Lower high frequency sideband (f2=43.4221 MHz)			
# FSR offset	l+m	offset from resonance	offset from anti-resonance
−1158	0	**16.26** kHz	**2499** Hz
−1158	1	16.21 kHz	
−1159	1		2550 Hz
−1159	2	11.16 kHz	
−1160	3	6.107 kHz	
−1161	4	**1.057** kHz	
−1162	5	3.992 kHz	
−1163	6	9.042 kHz	

Table 4: Table showing the closest sideband resonances in the arm cavities up to spatial modes with $l + m = 6$. Separation from exact anti-resonance is shown in column 4 if it is closer than 7 kHz. All offsets less than 2 kHz are highlighted in red, and the offsets of the $l + m = 0$ mode are highlighted in blue. This table is for the folded interferometers.

2.2 Optics properties and layout

2.2.1 Finesse and PRM transmission

We aim at an arm finesse of about 450, requiring an ITM transmission of $T_{ITM} = 0.014$. The finesse was lowered to this for a variety of reason, see "Arm Cavity Finesse for Advanced LIGO", LIGO-T070303. Assuming a loss of 37.5ppm per mirror ([2]) implies critical coupling at a Power Recycling mirror transmission of $T_{PRM}^{\text{crit}} = 0.023$. With $T_{PRM} = 0.03$ we aim for slight over-coupling (2% of carrier power reflected for nominal scattering loss, Figure 4). This both provides some robustness against the uncertainty in scatter loss, and - assuming

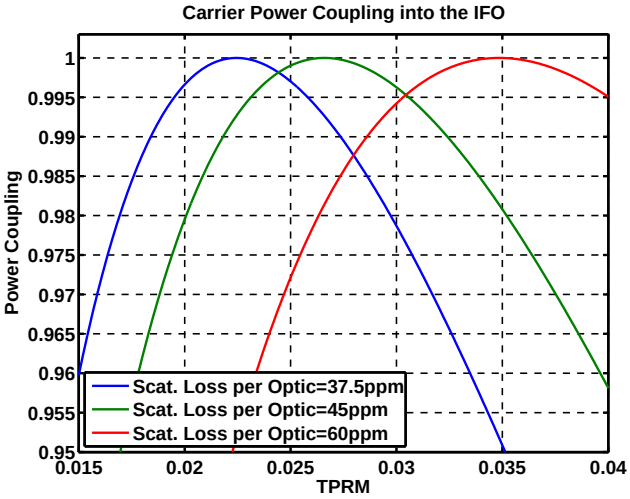

Figure 4: Carrier Power Coupling vs. T_{PRM} for a scatter loss of 37.5ppm, 45ppm and 60ppm per optic.

we correctly estimated the scatter loss - provides alternative and potentially better error signals for MICH and SRCL at the REFL port.

2.2.2 SRM transmission

The Signal Recycling mirror transmission can be chosen to optimize the bottom-line sensitivity. The test mass thermal noise is limiting over a broad frequency band. Thus we don't get any benefit from a narrow-band SRC, but are instead pushed to a low SRC finesse, meaning a high T_{SRM}. For NS/NS inspirals this results in $T_{SRM} = 0.16$ for the detuned case (Science mode 2), and in $T_{SRM} = 0.26$ for zero detuning (Science mode 1). However, as long as we are in the low finesse regime, it is not a very critical parameter. The sensitivity only depends weakly on T_{SRM}. We thus chose a round $T_{SRM} = 0.2$, which allows to come within about 1% of the optima for each science mode. All the Signal Recycling mirror transmission tuning was done in *bench62.m*.

2.2.3 Schnupp Asymmetry

The Schnupp Asymmetry was chosen to get close to critical coupling for the f_2 sideband in the dual recycling cavity. This condition maximizes the f_2 sideband power in the signal

recycling cavity. Note that, given T_{PRM} and T_{SRM}, there are two solutions for critical coupling the dual recycling cavity:

1. Small Schnupp Asymmetry, $l_{asy} \approx 4$ cm, $T_{asy} \approx 1.5e-3$: This requires that both Power and Signal Recycling Cavity are resonant for f_2.

2. Large Schnupp Asymmetry, $l_{asy} \approx 0.68$ m, $T_{asy} \approx 0.39$ This requires that exactly one of the two recycling cavities is resonant for f_2. The other one has to be anti-resonant.

Both solutions result in the same f_2 sideband power inside the Signal Recycling Cavity, but they generally result different sensing matrices.

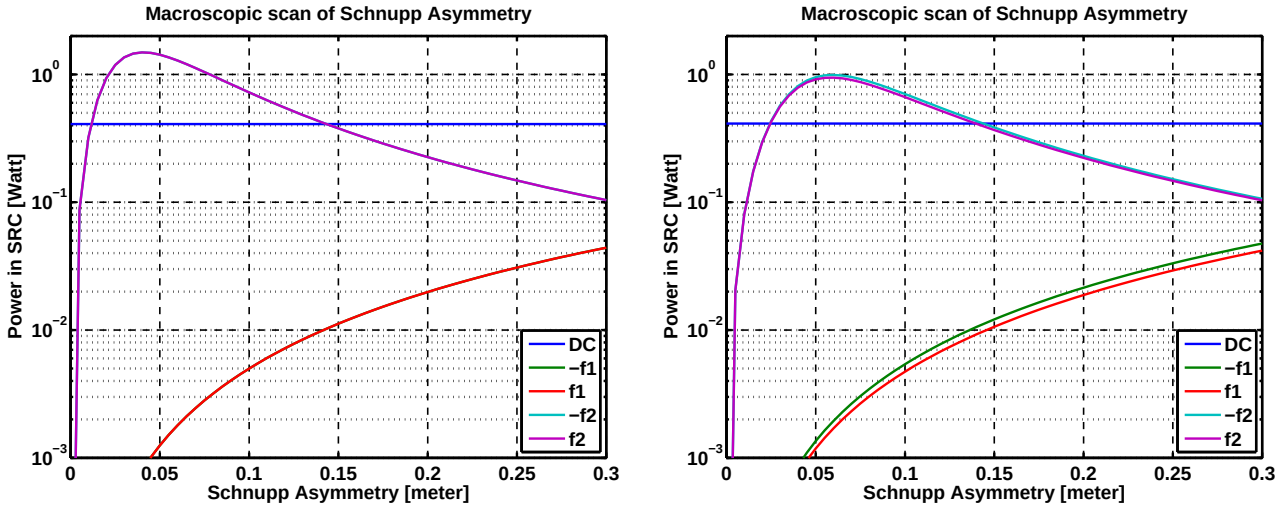

Figure 5: Power in Signal Recycling Cavity vs. Schnupp Asymmetry $l_{asy} = l_x - l_y$. The left plot is for zero SRM detuning (Science Mode 1), the right one is for the 11 deg detuning required for NS/NS tuning (Science Mode 2). Both recycling cavities are resonant for f_2, so the plot only shows the small Schnupp Asymmetry solution.

We chose the small Schnupp asymmetry (l_{asy}) because it allows a f1 to f2 sideband power ratio of 10^{-3} in the SRC, while the large l_{asy} only allows for about 10^{-1}. Thus the small l_{asy} provides a cleaner PRC / SRC separation in the error signals. Figure 5 also shows that the optimal Schnupp asymmetry changes from 4 cm to about 6 cm if we go to 11 deg SRM detuning.

Setting the Schnupp asymmetry to 5 cm is a good compromise between the two cases.

2.2.4 Power and Signal Recycling Cavity length

The Power Recycling Cavity has to be resonant for the f_1 and f_2 sideband when the arms are locked, i.e

$$l_{PRC} = (N + \frac{1}{2})\frac{c}{2f_1} \tag{2.1}$$

For a stable recycling cavity $l_{PRC} = 57.6557$ meters, $(N = 3)$ and $l_{PRC} = 60.4112$ meters, $(N = 3)$ are consistent with the opto-mechanical layout for the non-folded and folded interferometers.

The signal recycling has to be close to resonant for the f_2 sideband, while the f1 sideband is non-resonant.

$$l_{SRC} = M\frac{c}{2f_2}, \text{ but not } Q\frac{c}{2f_1} \tag{2.2}$$

M and Q integers. Figure 6 shows a macroscopic scan of the signal recycling cavity. For the non-folded IFOs we choose $l_{SRC} = 56.0084$ $(M = 17)$, while the folded IFO the opto-mechanical constraints suggest $l_{SRC} = 62.1372$ $(M = 18)$. Equation 2.2 should be met with a precision better than about 1 cm. This is because the relative demod angle of SRCL and MICH in the REFL double demod signal is exactly 90 deg and changes at a rate of about 9 deg per centimeter of offset from the resonance condition.

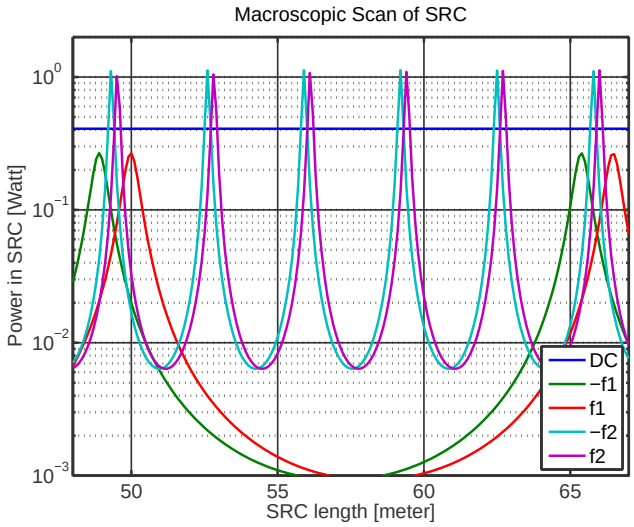

Figure 6: Power in Signal Recycling Cavity vs. Signal Recycling Cavity length for the non-folded interferometer and a detuned SRM (Science mode 2).

2.2.5 DC readout and DARM fringe offset

Loss difference in the arms and any asymmetry in the BS results in some light on the AS_DC photo diode even when the DARM offset is zero. Assuming a differential arm round trip loss of 30 ppm this light is on the order of $P_0 = 1$ mWatt (4 mWatt for 60 ppm, see figure 7).

The AS_DC light due to DARM offset is quadratic in DARM offset and reaches $P_{\mathrm{DARM}} =$ 100 mWatt at a DARM offset of about 12 pm (figure 7). 100 mWatt is also what we think our DC photo diode should be able to handle.

The homodyne phase is defined as the arctan (P_{DARM}/P_0). Theoretically the NS/NS range peaks at a homodyne phase somewhere around 100 deg, but the sensitivity gain compared to a homodyne phase of 90 deg is minimal. Also technical noise couplings such as Intensity noise become bigger for small DARM offsets, thus driving us to larger offsets (i.e. closer

to 90 deg homodyne phase). Thus we most likely will operate at a DARM offset of about 10 pm.

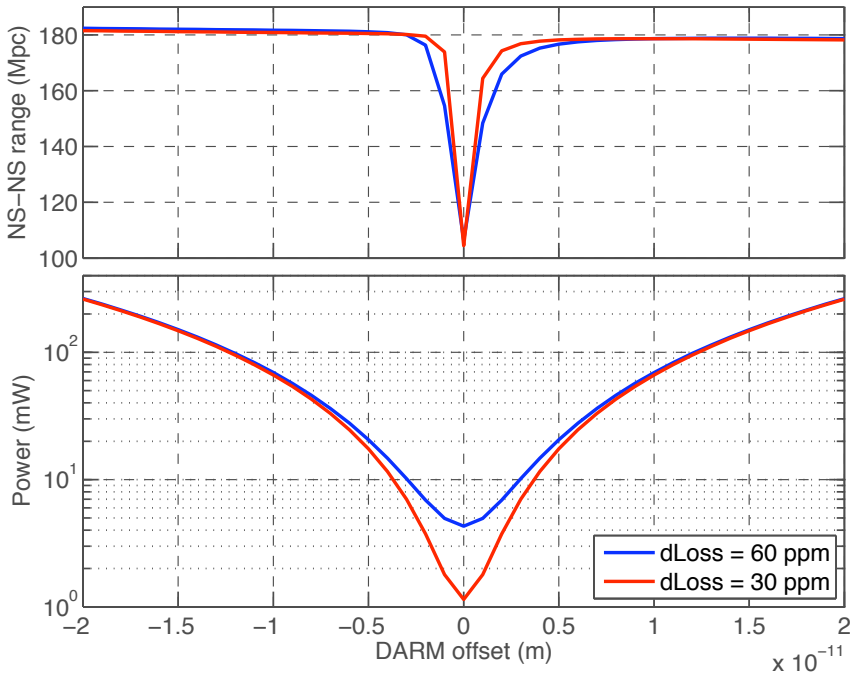

Figure 7: Sensitivity and AS DC power as a function of DARM offset. Here the sensitivity only includes contribution from Quatum noise and mirror thermal noise.

2.3 Error signals

In addition to AS DC, length error signals are derived from demodulating the REFL and POX beam at f_1, f_2, $f_2 + f_1$ and $f_2 - f_1$. For primary feedback we will use REFL I1 for CARM (high bandwidth analog loop), AS DC for DARM, and POP I1 for PRCL, POP Q2 for MICH. The best SRCL error signal depends on the detuning. For Science mode 1 (zero detuning) we chose REFL I2. POB I2 would also be an option. For Science mode 2 (NS/NS detuning) REFL IM/IP is the better choice, but this doesn't work for zero detuning. The sensing matrix for these ports is given in section 3.1.

In appendix A, Table 7 shows the the full sensing matrix for the detuned case, while Table 8 shows the Non-detuned case. The dominant matrix elements are highlighted in red.

Figure 8 shows how the different SRCL error signals depend on the signal recycling detuning. After CARM and DARM are locked, the transfer functions from SRCL to both REFL I2 and POP I2 are basically flat and only vary in overall gain according to the (derivative) of Figure 8.

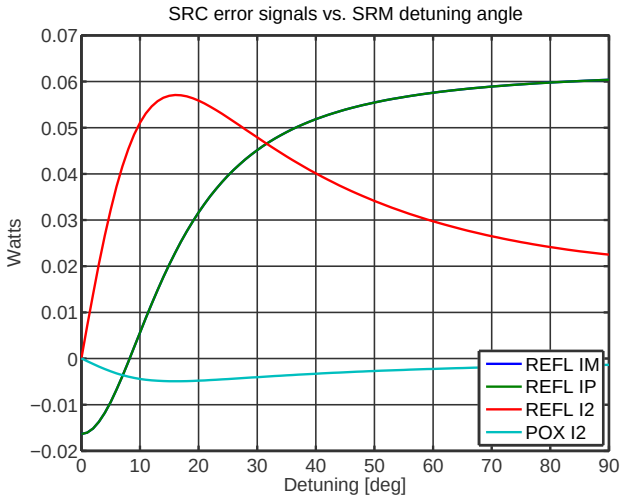

Figure 8: SRC error signals vs SRM detuning angle. Switching between REFL IM/IP and REFL I2/POX I2 at a detuning angle of about 5 deg allows for continuous detuning to any desired phase. POB looks identical to POX.

2.4 Optical power at sensing ports

The tables below show the power exiting the back side of the power recycling mirror (PRM) and signal recycling mirror (SRM) (labeled IFO_REFL and IFO_AS respectively), as well as the power at each optical sensing port in mWatt. The ports REFL, POP and OMCR were attenuated to 100 mWatt. Note that AS_DC is the OMC transmitted port. The frequencies are for the non-folded interferometers. 24.1 MHz is the mode cleaner modulation frequency.

Optical Port Power in mWatt for mode 1 (zero detuning)

FREQ (MHz)	-54.6	-45.5	-36.4	-24.1	-9.1	0.0	9.1	24.1	36.4	45.5	54.6	Total
IFO_REFL	0.8	8.5	0.8	0.0	245	1434	245	0.0	0.8	8.5	0.8	1945
IFO_AS	0.0	290.0	0.0	0.0	0.2	79.9	0.2	0.0	0.0	290.0	0.0	660
REFL	0.0	0.4	0.0	0.0	12.6	73.8	12.6	0.0	0.0	0.4	0.0	100
AS_DC	0.0	0.1	0.0	0.0	0.0	79.9	0.0	0.0	0.0	0.1	0.0	80
POP	0.0	0.1	0.0	0.0	0.7	98.3	0.7	0.0	0.0	0.1	0.0	100
OMCR	0.0	50.0	0.0	0.0	0.0	0.0	0.0	0.0	0.0	50.0	0.0	100
IMC	0.0	0.1	0.0	29.0	0.1	22.1	0.1	29.0	0.0	0.1	0.0	80

Optical Port Power in mWatt for mode 2 (detuned)

FREQ (MHz)	-54.6	-45.5	-36.4	-24.1	-9.1	0.0	9.1	24.1	36.4	45.5	54.6	Total
IFO_REFL	0.8	108.7	0.8	0.0	245	1430	245	0.0	0.8	96.3	0.8	2129
IFO_AS	0.0	170.3	0.0	0.0	0.2	80.7	0.2	0.0	0.0	179.7	0.0	431
REFL	0.0	5.1	0.0	0.0	11.5	67.2	11.5	0.0	0.0	4.5	0.0	100
AS_DC	0.0	0.0	0.0	0.0	0.0	80.7	0.0	0.0	0.0	0.0	0.0	81
POP	0.0	0.4	0.0	0.0	0.7	97.9	0.7	0.0	0.0	0.4	0.0	100
OMCR	0.0	48.6	0.0	0.0	0.1	0.0	0.1	0.0	0.0	51.3	0.0	100
IMC	0.0	0.1	0.0	29.0	0.1	22.1	0.1	29.0	0.0	0.1	0.0	80

2.5 (Electrical) RF power at sensing ports

Finally, the two tables below show the RF signal level at the relevant frequencies for the REFL and POP port. The signals are still in mWatt - multiply with the photodiode gain of $\epsilon \cdot 0.86$ Ampere/Watt to get Amperes. ϵ is the quantum efficiency. The reported values include both quadratures.

RF power at ports in mWatt for zero-detuned operation (science mode 1)

FREQ (MHz)	0.0	9.1	18.2	36.4	45.5	54.6	91.0
REFL	90.14	0.08	20.19	21.58	0.04	19.37	7.05
POP2	99.89	0.00	1.43	1.13	0.00	1.13	0.22

RF power at ports in mWatt for detuned operation (science mode 2)

FREQ (MHz)	0.0	9.1	18.2	36.4	45.5	54.6	91.0
REFL	99.95	0.09	20.19	34.43	26.06	31.99	16.85
POP	100.01	0.00	1.43	1.41	4.14	1.41	0.33

3 Science mode length and frequency controls

The sensing matrix and noise at each port were calculated using the AdvLIGO Optickle and Looptickle model (see appendix C). These calculations used the old set of parameters given in table 6.

The following table summarizes the main features of the control loops:

Loop	*Error signal*	*UGF*	*Phase margin*
CARM	REFL_I1	65 kHz	68 deg
DARM	AS_DC	446 Hz	26 deg
PRCL	POP_I1	21 Hz	32 deg
MICH	POP_Q2	20 Hz	34 deg
SRCL	REFL_IM / REFL_IP	15 Hz	37 deg
IMCL	IMC_I3	377 kHz	68 deg

The table is for the NS/NS case. In the zero detuning case the SRCL loop uses POP_I2 or REFL_I2 as error signal.

The SRCL→DARM and MICH→DARM correction paths were implemented as described in paragraph 3.5 with an accuracy of about 1%. Additionally a very rough PRCL→DARM correction path was also implemented about 10% precision.

3.1 Sensing matrix

The following sensing matrices for Science mode 1 and 2 were calculated in Optickle:

Sensing Matrix in Watts per meter at 1 kHz, for Science Mode 2 (NS/NS inspiral)

Port	CARM	DARM	PRCL	MICH	SRCL
REFL I1	**9.4e+08**	2e+05	7.3e+07	1.1e+06	**5.5e+03**
AS DC	1.3e+06	**4.2e+09**	2.8e+05	1.5e+07	7.6e+06
POP I1	3.2e+07	6.7e+03	**1.2e+07**	**6.8e+03**	**3.1e+02**
POP Q2	1.5e+07	2.3e+04	**1.4e+06**	**4.3e+05**	**3e+04**
REFL IM	1.4e+06	**2.5e+04**	**5.1e+06**	**4.5e+05**	**2.8e+05**

Sensing Matrix in Watts per meter at 1 kHz, for Science Mode 1 (zero detuning)

Port	CARM	DARM	PRCL	MICH	SRCL
REFL I1	**9.4e+08**	1.3e+05	7.3e+07	1e+06	**1.4e+04**
AS DC	3e+06	**9.7e+09**	6.7e+05	3.4e+07	7e+03
POP I1	3.2e+07	4.4e+03	**1.2e+07**	**6.6e+03**	**3e+02**
POP Q2	8.7e+06	4.2e+04	**4.6e+05**	**7.4e+05**	**8.8e+04**
POP I2	8.7e+06	9e+03	**1.8e+06**	**9.9e+04**	**3e+05**

The contractions used in the port name are: I: I-phase, Q: Q-phase, 1: demodulated at f_1, 2: demodulated at f_2, M: demodulated at $f_2 - f_1$, P: demodulated at $f_2 + f_1$. The main matrix elements are in bold red. The biggest worrisome elements are in blue. The full sensing matrix with all available ports is shown in Figures 7 and 8 of appendix A.

3.2 Sensing noise

The shot noise for 100 mWatt on the detection diodes the shot noise is about $2e{-}10$ Watt/$\sqrt{\text{Hz}}$; it varies slightly between the ports because the non-stationary shot noise contribution depends on the amount of sideband. The following table summarizes the optical gain and approx. sensing noise at 100Hz. It is calculated for science mode 2 (NS/NS), but the numbers for zero-detuning are very similar. (See also sections 3.3 and 3.4 for detailed noise budgets.)

Loop	*Port*	*optical gain at 100 Hz*	*sensing noise at 100 Hz*
CARM	REFL_I1	$8.5e+10$ m/Watt	$2.4e-21$ m/$\sqrt{\text{Hz}}$ (*)
DARM	AS_DC	$2.1e+10$ m/Watt	$9.5e-21$ m/$\sqrt{\text{Hz}}$
PRCL	POP_I1	$1.2e+7$ m/Watt	$1.7e-17$ m/$\sqrt{\text{Hz}}$
MICH	POP_Q2	$4.4e+5$ m/Watt	$4.5e-16$ m/$\sqrt{\text{Hz}}$
SRCL	REFL_IM	$2.9e+5$ m/Watt	$6.9e-16$ m/$\sqrt{\text{Hz}}$

(*): Because MC2 is the actuation point of the CARM loop, it's number is in meters of MC2 motion. Multiply by l_{arm}/l_{MC} for meters of CARM.

3.3 DARM noise budget

The various noise budgets below contain the following noise sources:

- **Quantum** or **Shot Noise** from the loop itself, calculated by injecting vacuum noise at every open optical port.

- **Shot Noise** from the other loops, calculated by propagating the quantum noise in the other loops through the control system.
- **Seismic Noise**, using the expected performance of the ISI and Quad suspension. Currently only the seismic noise of the 4 test mass suspensions is included.
- **Thermal Noise**, including Mirror Thermal and Suspension Thermal noise.
- **Frequency Noise** incident on the input mode cleaner (i.e. input mode cleaner and common mode sensing noise are counted as shot noise from those length loops). The used numbers are 1 Hz/rtHz at and below 20Hz, $2e-2$ Hz/rtHz at and above 1000Hz.
- **Intensity Noise** incident on the IMC. The used numbers are $2e-9$ 1/rtHz at and below 10Hz, $1e-7$ Hz/rtHz at and above 500Hz.
- **Oscillator Phase Noise**, using the specification of a Wenzel Crystal Oscillator ($1e-5$ rad/rtHz at and below 10Hz, $3e-7$ rad/rtHz at 100Hz, $2e-8$ rad/rtHz at and above 1000Hz). The coupling does include the light passing through the IMC. Currently the estimate does not include potential noise added after the EOM/LO split.
- **Oscillator Amplitude Noise**, using the specification of a Wenzel Crystal Oscillator ($1e-7$ rad/rtHz at and below 10Hz, $1e-8$ rad/rtHz at 100Hz, $3e-9$ rad/rtHz at and above 1000Hz).
- **Facility** includes Gravity Gradient noise and residual gas noise.

Arguably the most important noise source that is missing in these budgets is the cross-coupling from angular control loops. See the ASC design document [**?**] for more details.

The DARM noise budget for the NS/NS case is shown in figure 9, the zero-detuning case is shown in figure 10.

3.4 Auxiliary loops noise budget

The figures 11 to 15 show noise budgets for all auxiliary loops. For SRCL and MICH both the NS/NS and zero-detuning cases are shown (figures 11,12,15, and 16).

3.5 Required correction paths

The in-band noise of all auxiliary loops is sensing-noise limited, i.e the control system adds displacement noise to the auxiliary optics at the frequencies we care. This extra noise then couples to DARM through known mechanisms.

But since this coupling is known it is possible to cancel the noise by also sending a filtered copy of the auxiliary loop control signals to the ETMs, see figure 17.

The dominant coupling mechanisms are:

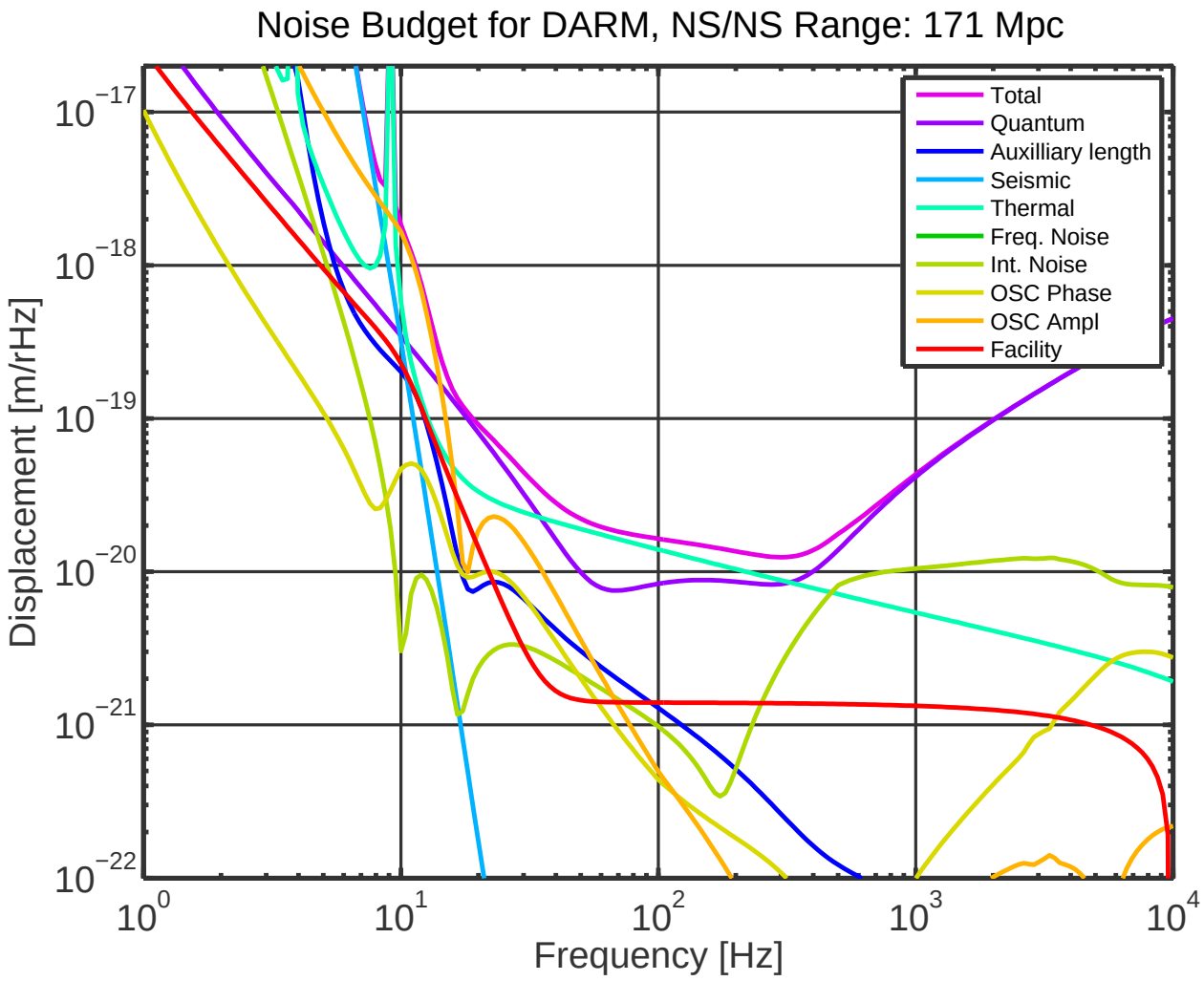

Figure 9: DARM noise budget for the NS/NS case.

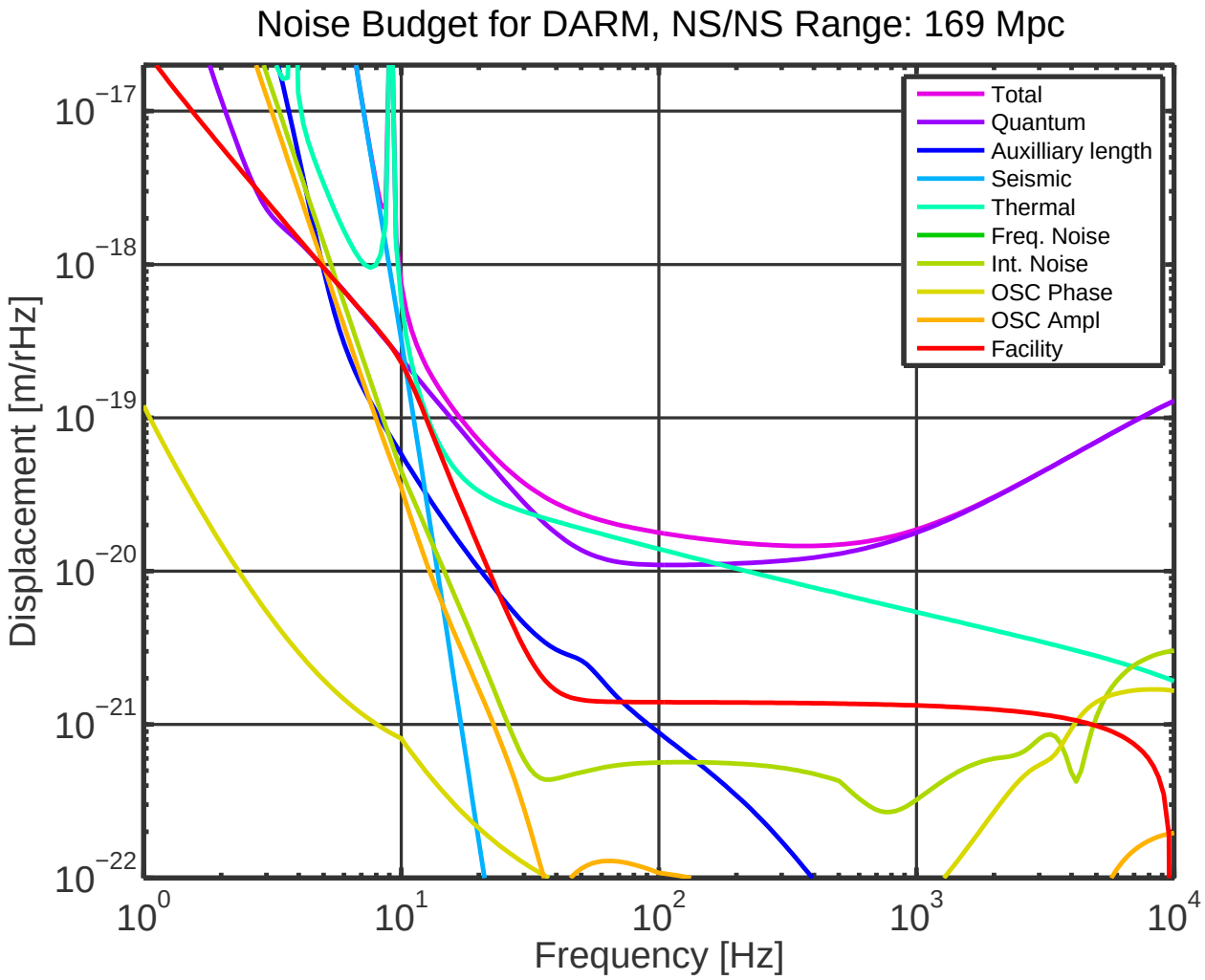

Figure 10: DARM noise budget for the zero detuning case.

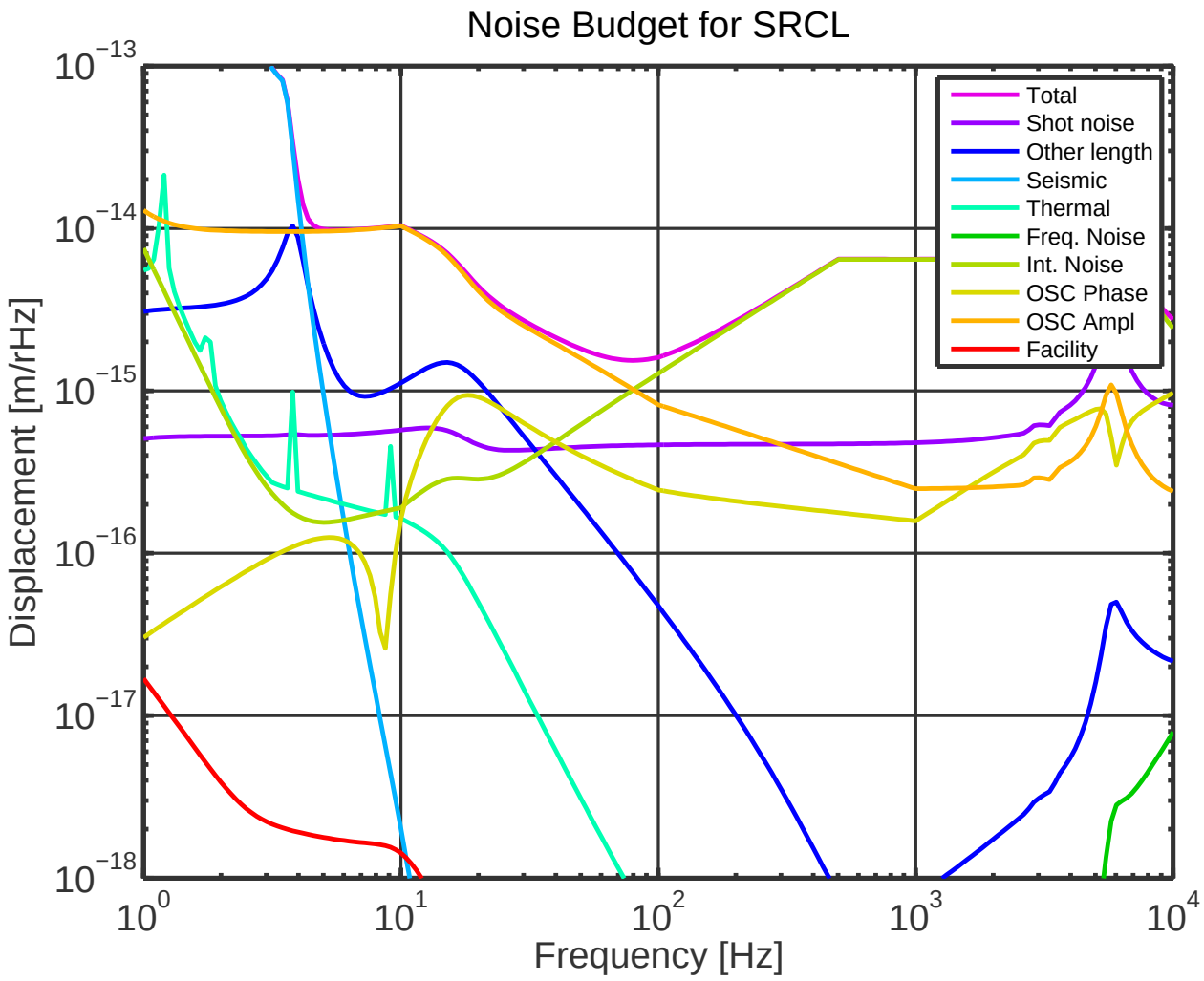

Figure 11: SRCL noise budget for the NS/NS case.

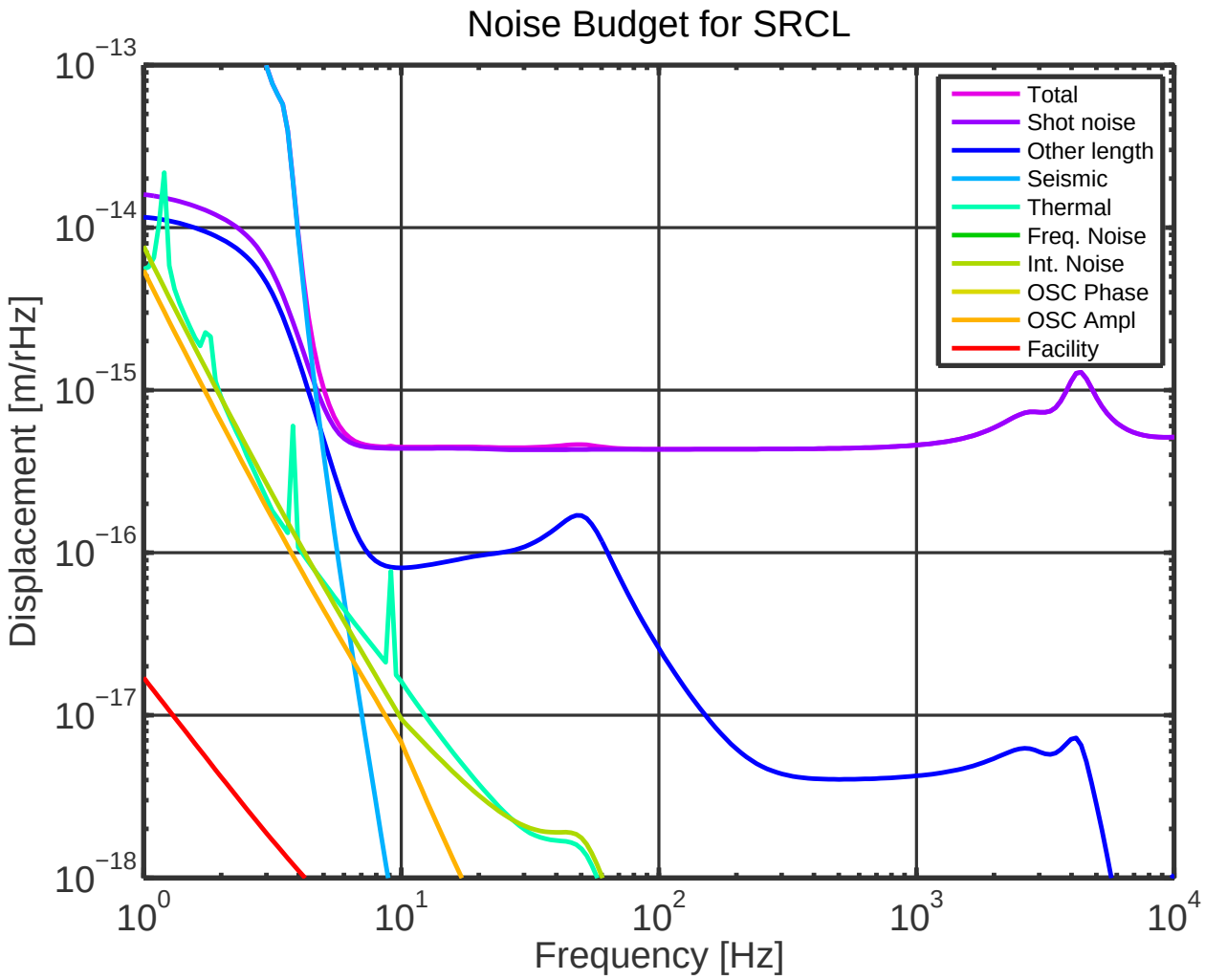

Figure 12: SRCL noise budget for the zero detuning case.

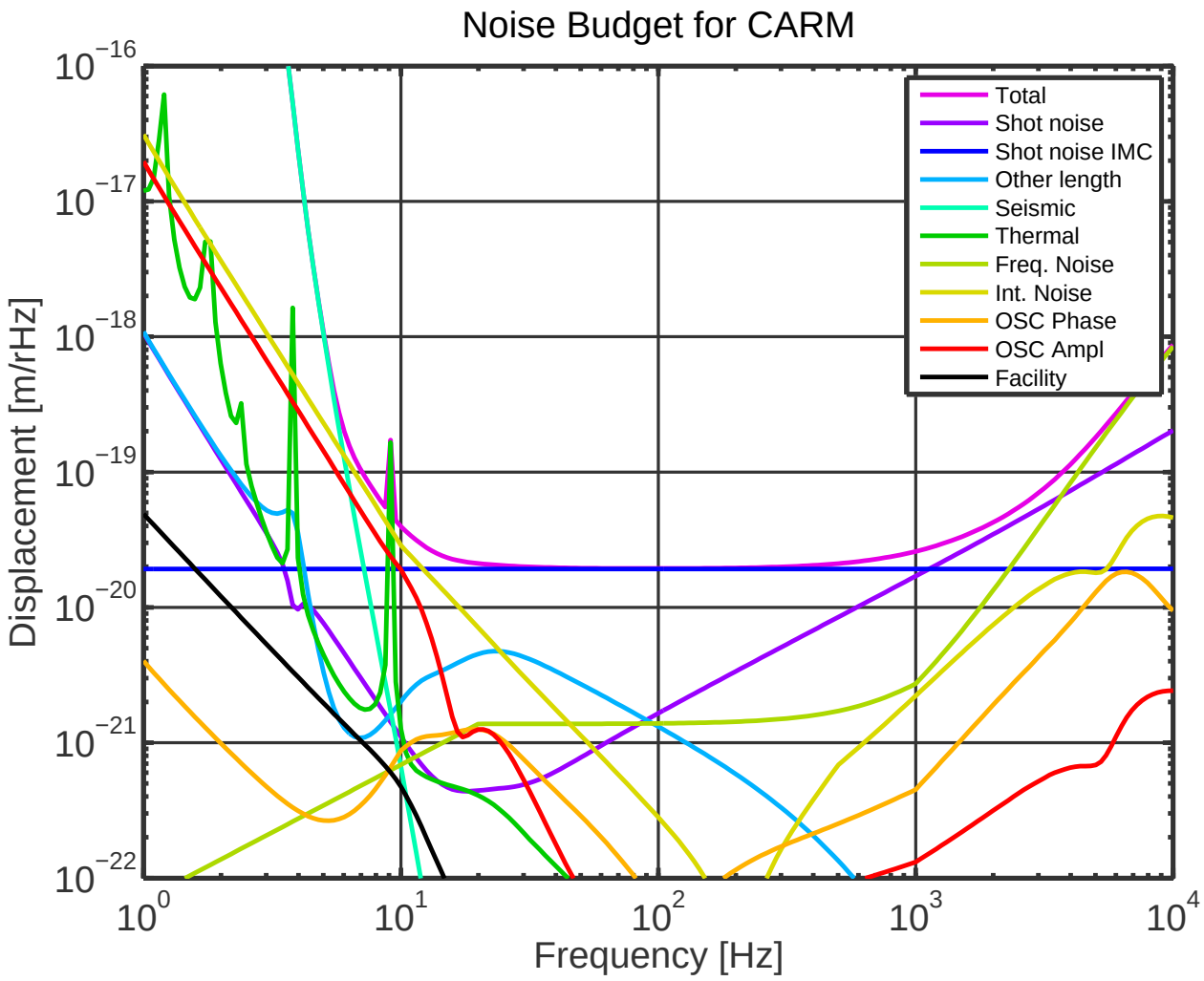

Figure 13: CARM noise budget for the NS/NS case.

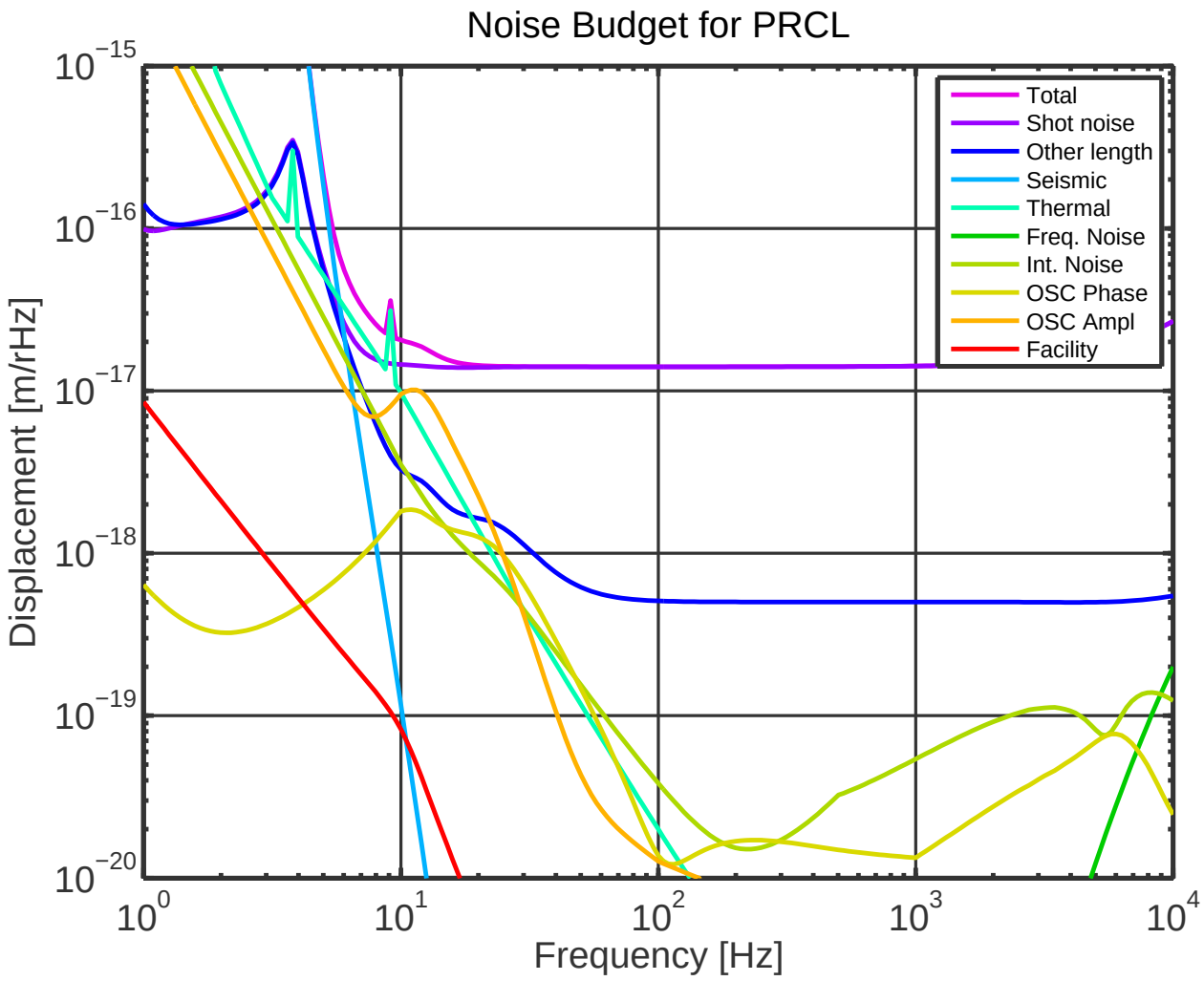

Figure 14: PRCL noise budget for the NS/NS case.

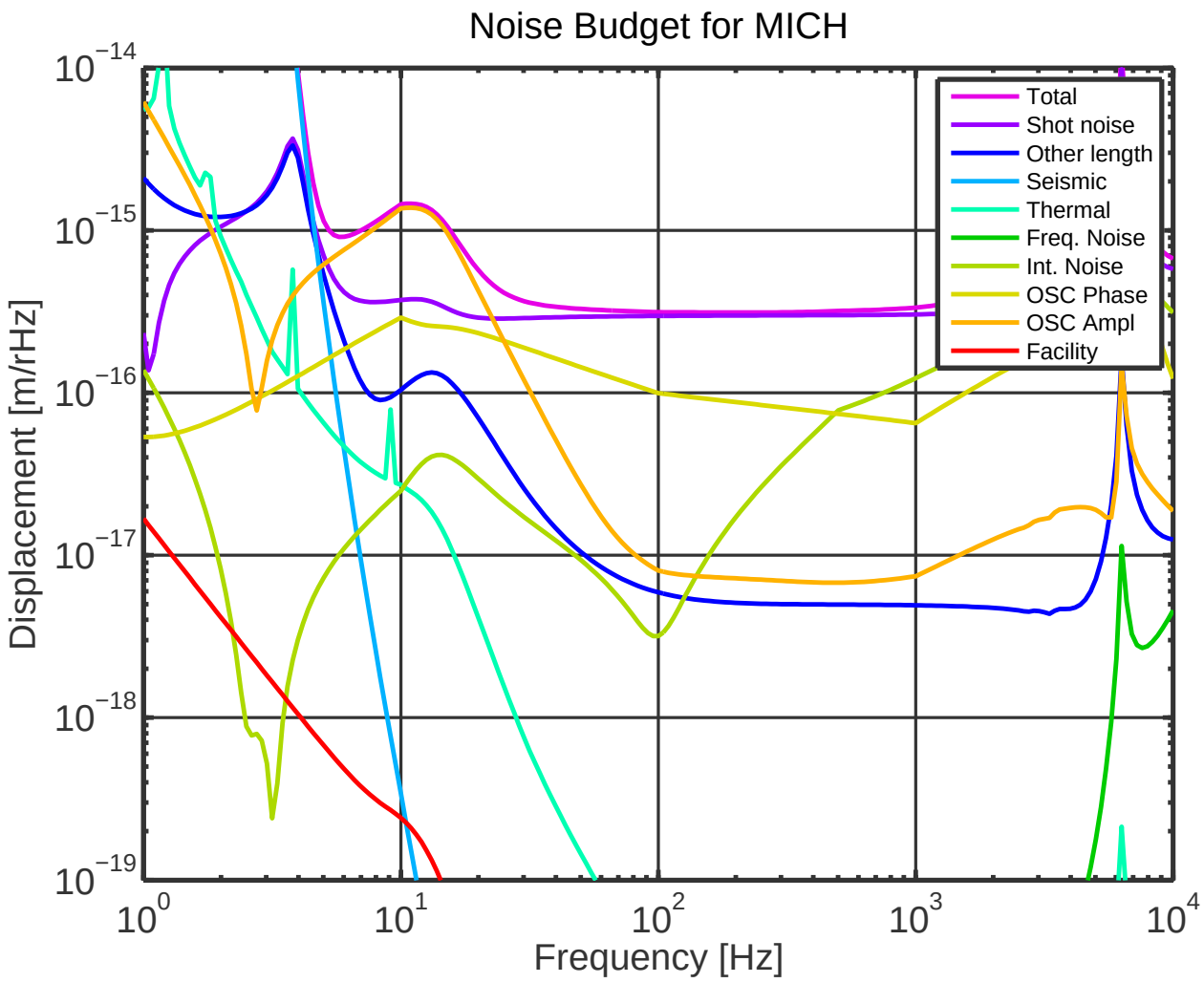

Figure 15: MICH noise budget for the NS/NS case.

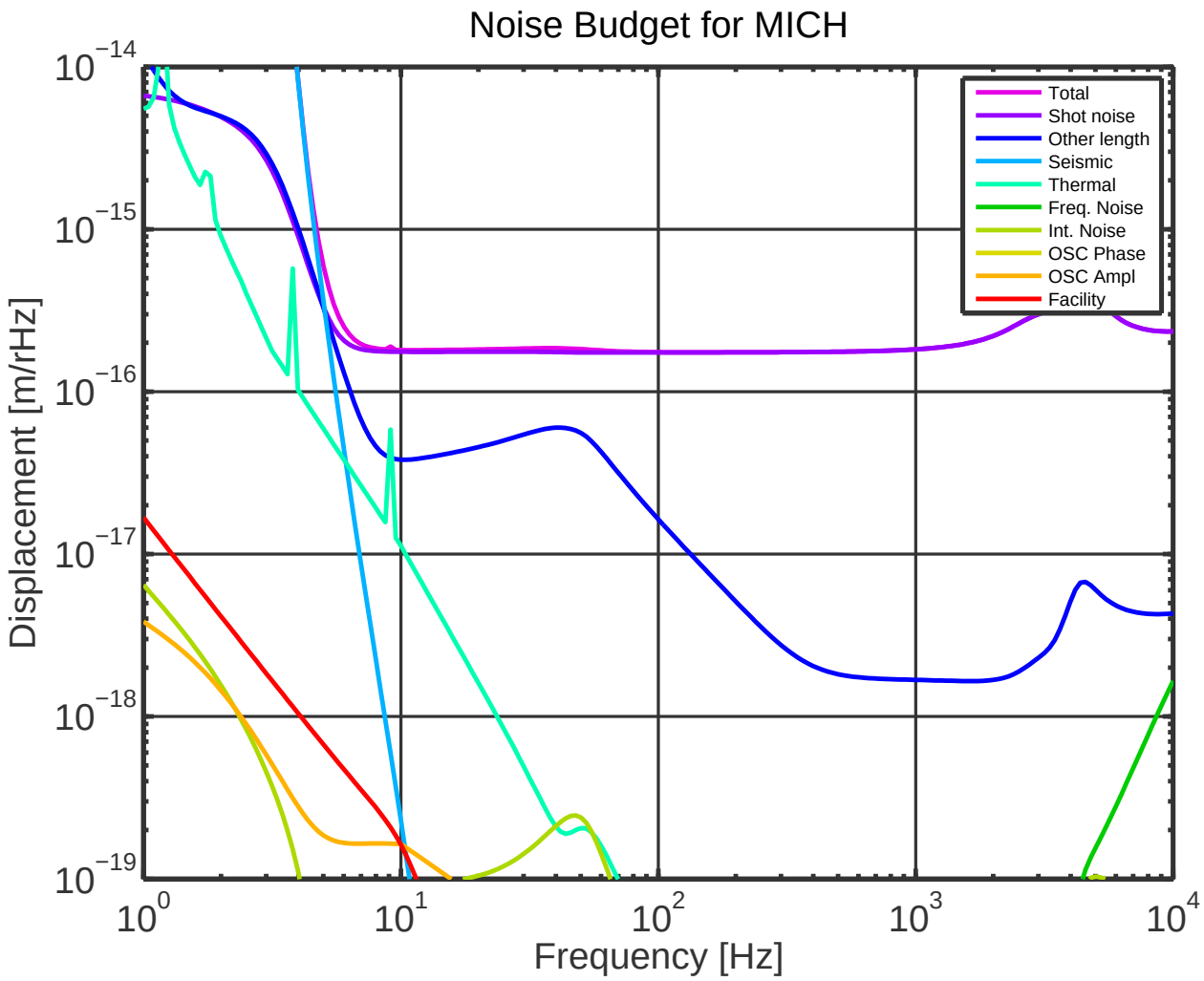

Figure 16: MICH noise budget for the zero detuning case.

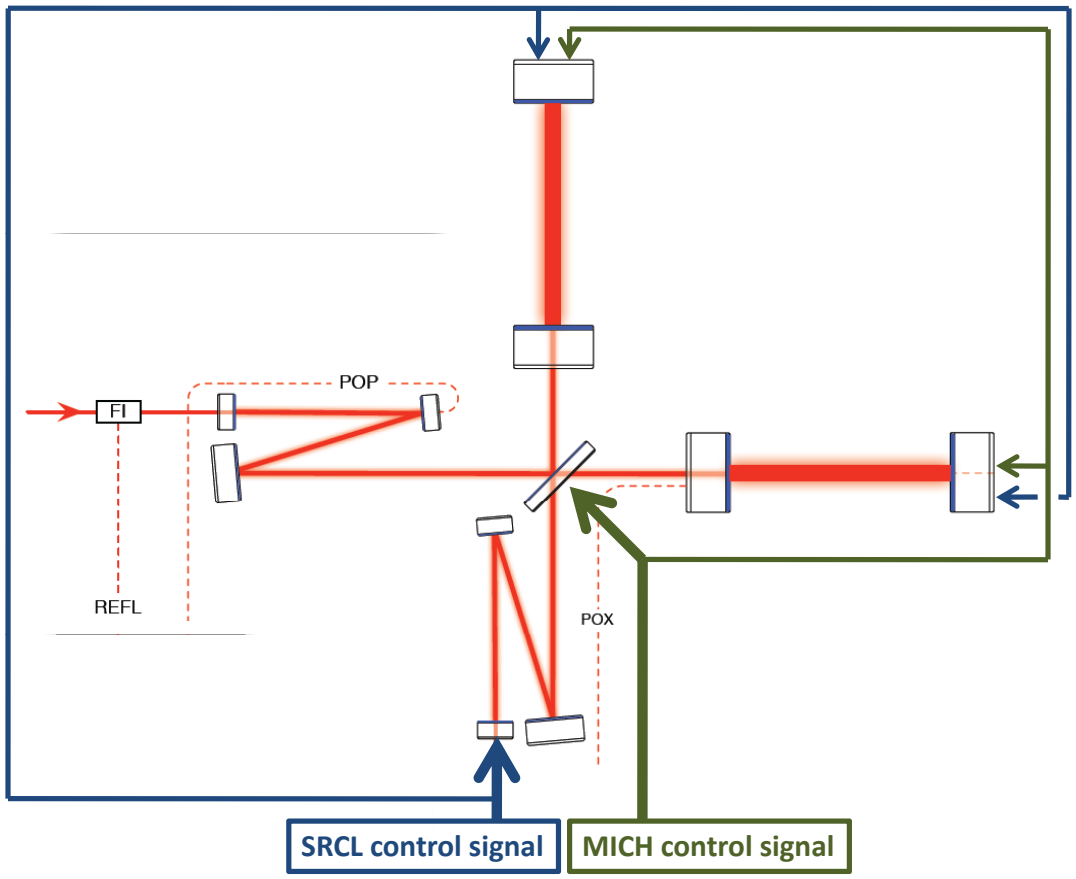

Figure 17: MICH and SRCL correction paths. A filtered copy of the sensing noise limited MICH and SRCL control signals is sent to the ETMs to cancel known couplings.

Loop	*Port*	*Fringe offset*
DARM	AS_DC	$1.5e-15$ m rms
PRCL	POP_I1	$4.5e-12$ m rms
MICH	POP_Q2	$1.8e-11$ m rms
SRCL	REFL_IM	$3.1e-12$ m rms

Table 5: RMS fringe offset for the main control loops. All loops are dominated by the micro-seism. No resonant gain filters have been applied so far.

- MICH coupling: It's coupling in DARM meters per MICH meters is given by

$$K_{\mathrm{MICH}} = \frac{\pi}{2F}, \tag{3.1}$$

  where F is the arm finesse. One MICH correction path with a precision of about 1% is needed.

- SRCL coupling: The SRCL to DARM coupling is not only the dominant coupling path for SRCL sensing noise, but also for other noise sources, such as PRCL sensing noise, intensity noise and oscillator phase noise. It's shape consists of two parts. At low frequency the coupling is dominated by radiation pressure and can be parametrized as

$$K^{(1)}_{\mathrm{SRCL}} = 0.012 \left(\frac{10\ \mathrm{Hz}}{f}\right)^2 \left(\frac{P_{\mathrm{arm}}}{750\ \mathrm{kW}}\right) \left(\frac{0.014}{T_{ITM}}\right) \left(\frac{\mathrm{DARM_{offset}}}{10\ \mathrm{pm}}\right) \tag{3.2}$$

At high frequencies on the other hand the coupling is independent of power and approximately given by

$$K^{(2)}_{\mathrm{SRCL}} = 3 \cdot 10^{-5} \left(\frac{f}{100\ \mathrm{Hz}}\right)^2 \left(\frac{SRC_{\mathrm{detuning}}}{10\ \mathrm{degree}}\right) \left(\frac{0.014}{T_{ITM}}\right) \left(\frac{\mathrm{DARM_{offset}}}{10\ \mathrm{pm}}\right) \tag{3.3}$$

We therefore need two SRCL to DARM correction paths, one that scales with arm power, and another static one. Both need to be accurate to about 1%.

3.6 Error and control signal size

Using the Optickle and Loopticke model the in-loop (i.e. loop-suppressed) error signals were calculated and plotted in Figure 18.

Also, Figure 19 show the required drive to the test masses. It was calibrated in Newtons acing on a free, 40 kg test mass, i.e. the actuation details for the quad suspension were not included. The test mass was assumed to be 40 kg for all loops, even though the some mirrors are lighter.

Finally, table 5 show the residual fringe offset. DARM, PRCL, MICH and SRCL are all dominated by the micro-seism, but no resonant gain filters have been applied so far.

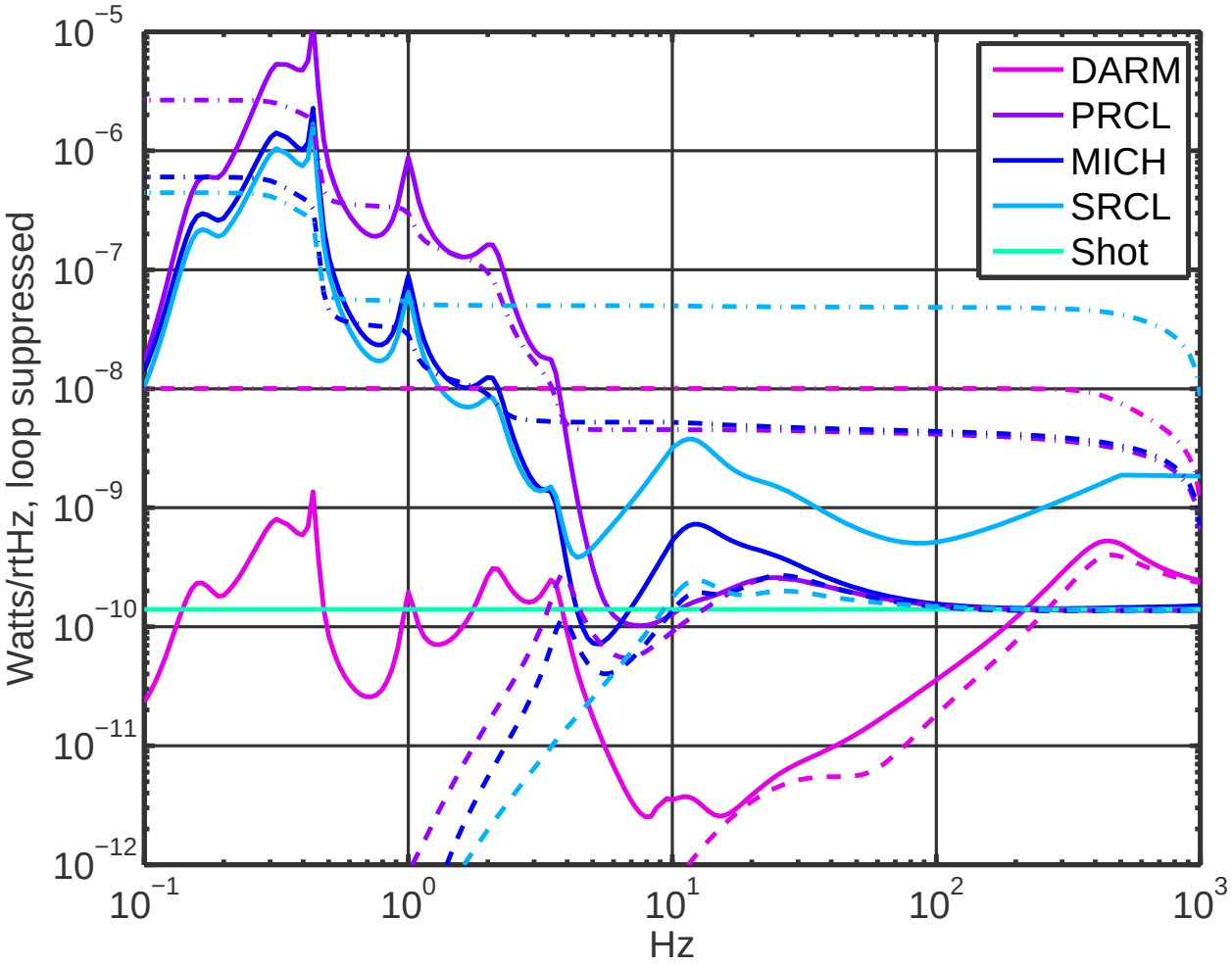

Figure 18: Error signals (loop-suppressed) for DARM, PRCL, MICH and SRCL. The corresponding RMS values (integrated from high to low frequency) are shown as dash-dot lines. The (loop-suppressed) quantum noise for each loop is shown as dashed lines. The (not loop-suppressed) sensing noise is indicated by the line labeled 'Shot'.

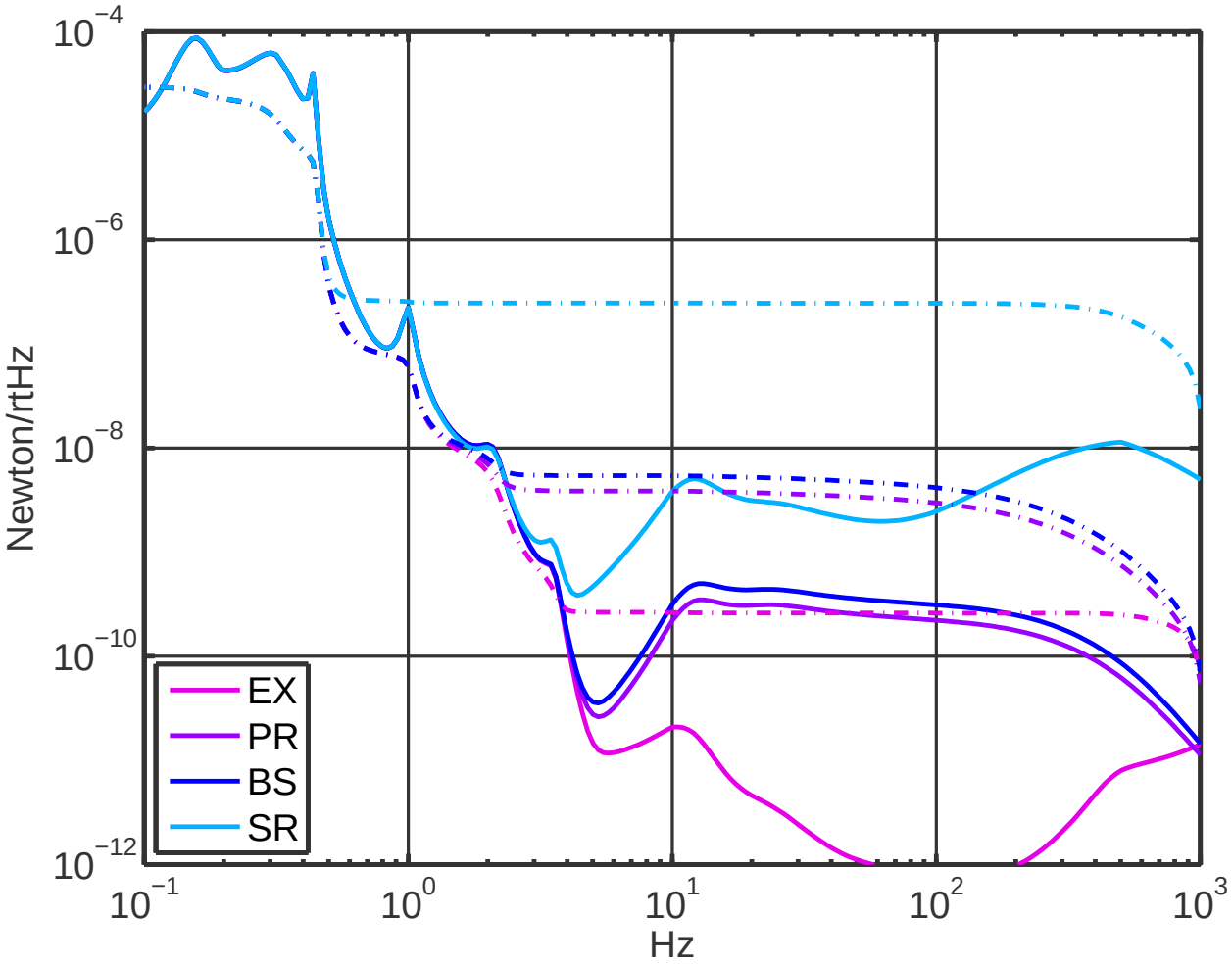

Figure 19: Control signals driving ETM, PR, BS and SR. All signals are calibrated in Newton at the test mass, assuming a free, 40 kg test mass (only appropriate for ETM). Since the actuation details for the quad suspension were not included, the low frequency part is not reliable. The corresponding RMS values (integrated from high to low frequency) are shown as dash-dot lines.

Quantity	*Non-Folded IFOs*	*Folded IFO*
Finesse	446	446
ITM transmission	0.014	0.014
PRM transmission	0.030	0.030
SRM transmission	0.200	0.200
Schnupp asymmetry	0.050	0.050
l_{PRC}	57.676 m	60.398 m
l_{SRC}	56.028 m	62.124 m
l_{IMC} (round trip)	32.957 m	34.513 m
l_{EX}	3994.75 m	3996.00 m
l_{EY}	3994.75 m	3996.00 m
Lower mod. frequency	9'096'270 Hz	8'686'280 Hz
Upper mod. frequency	45'481'350 Hz	43'431'400 Hz

Table 6: **Old** interferometer parameters for both folded and non-folded case. These parameters are still listed because they were were used for most of the Optickle simulation results. See 2 for actual parameters.

4 No Signal Recycling Mirror (No-SRM) Operation

4.1 No-SRM tuning

During early commissioning the Advanced LIGO interferometers will most likely be operated without signal recycling mirror (SRM). The Schnupp asymmetry was optimized to 5 cm assuming the presence of a SRM - see section 2.2.3 and figure 5. This value is not optimal (too small) for No-SRM operations.

A priori there are three options:

- Stay with 5 cm Schnupp asymmetry and $f2 = 5 \times f1 \approx 45$ MHz, but sacrifice some MICH sensing noise.
- Stay with 5 cm Schnupp asymmetry, and go to $11 \times f1 \approx 99$ MHz for optimal MICH sensing noise. A variant would be to go slightly up in frequency, say to $7 \times f1 \approx 63$ MHz.
- Stay at $f2 = 5 \times f1 \approx 45$ MHz, and increase the Schnupp asymmetry to 11cm for optimal MICH sensing noise. This is obviously complicated.

Figure 20 shows the No-SRM MICH sensing noise as a function of Schnupp asymmetry for the three cases "5xf1", "7xf1" and "11xf1". The sensitivity hit in MICH for the easiest case (5 cm and "5xf1") is only about 30%, so that is where we plan to operate.

Additionally figure 20 shows the problem of getting the $f2$ sideband too close to arm resonance. The trace "$5 \times f1$, arm res." corresponds to the No-SRM MICH sensitivity for the old design parameters (table 6). For those parameters the $f2$ sideband is 3.1 kHz away from arm resonance, which already produces a big enough arm reflection phase shift to degrade the MICH sensitivity by a factor of 4. The same problem is also illustrated in figure 3.

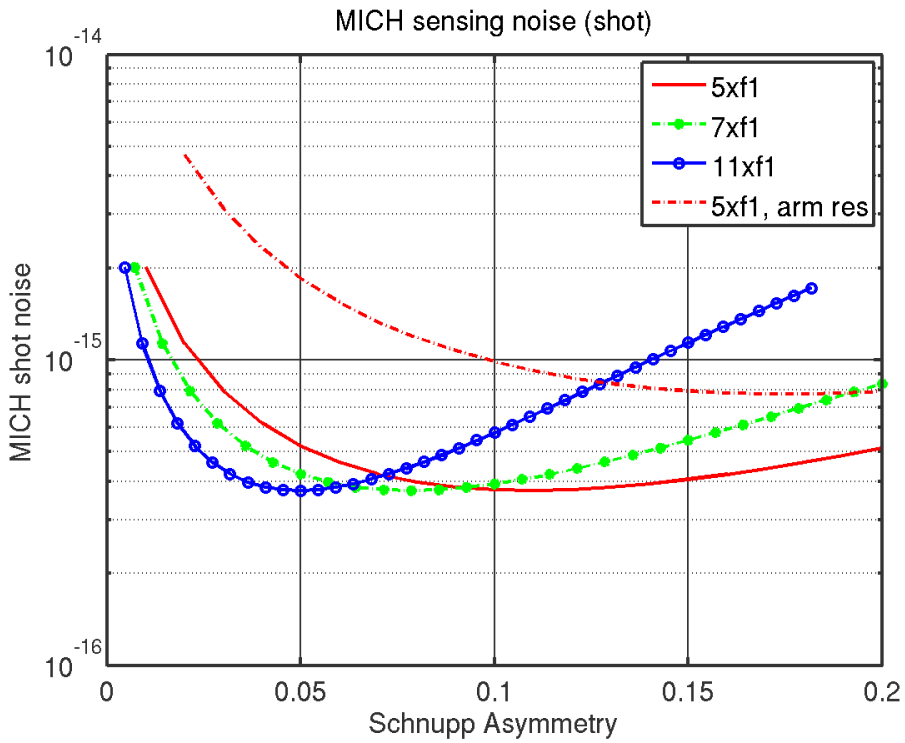

Figure 20: No-SRM MICH sensing noise as a function of Schnupp asymmetry for the three cases "5xf1", "7xf1" and "11xf1". Operating at 5 cm Schnupp asymmetry and with $f2 = 5 \times f1$ is feasible and only results in a 30% MICH sensing noise increase.

Finally figures 21, 22 and 23 are noise budgets for the DARM, MICH and PRCL degree of freedoms. They show that a shot noise sensitivity limited sensing of the auxiliary degrees of freedom is achievable for most of the frequency band of interest.

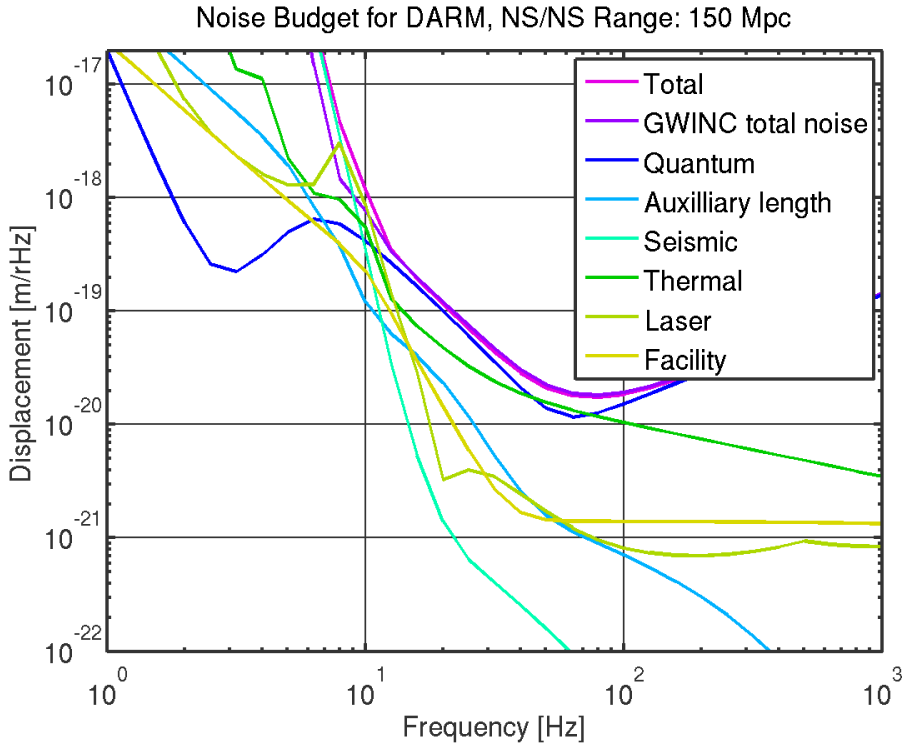

Figure 21: DARM noise budget for No-SRM (no signal recycling mirror) operation. The Schnupp asymmetry is left at 5 cm and $f2 = 5 \times f1$ is used for MICH sensing.

A Appendix: Full sensing matrix

Figures 7 and 8 show the full sensing matrix at 1 kHz for the NS/NS tuning and the zero-detuning case.

B Appendix: Sensing marix with and without Mach Zehnder

The following tables compare the sensing matrices with (table 9, 11, 13, 15) and without Mach Zehnder (table 10, 12, 14, 16) . They are calculated for the NS/NS (mode 2) (9, 10, 11, 12) and the no detuning case (mode 1b) (13, 14, 15, 16) , both at 20 Hz and 1 kHz. The only matrix elements that show a significant change are highlighted in magenta. The units for all matrices are Watts per meter.

Also figure 24 shows the REFL IM and IP double demodulation signal as a function of the SRC cavity detuning.

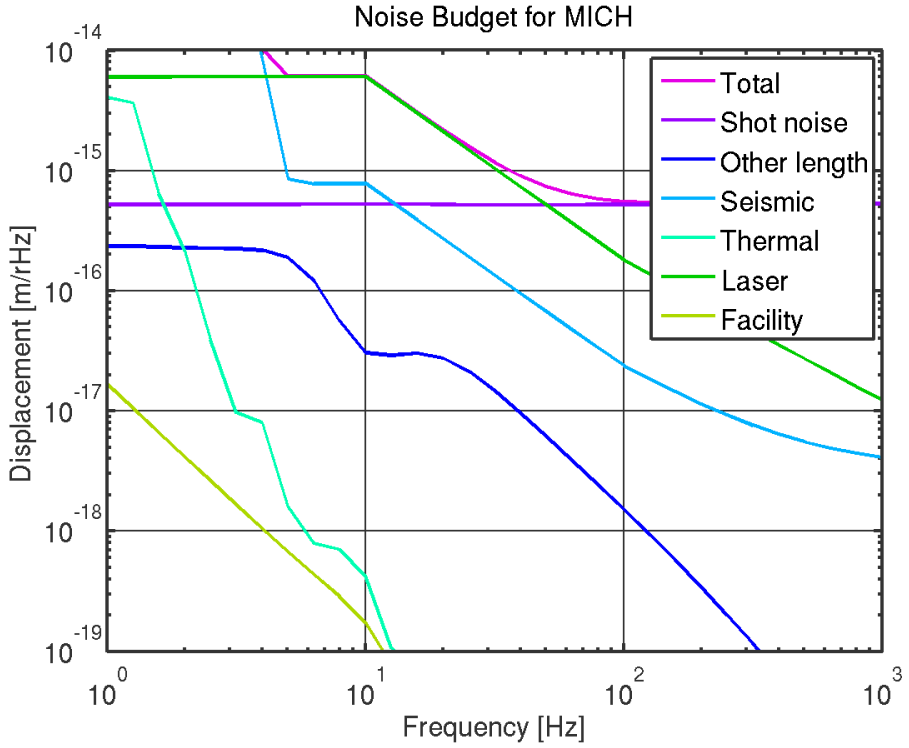

Figure 22: MICH noise budget for No-SRM (no signal recycling mirror) operation. The Schnupp asymmetry is left at 5 cm and $f2 = 5 \times f1$ is used for MICH sensing.

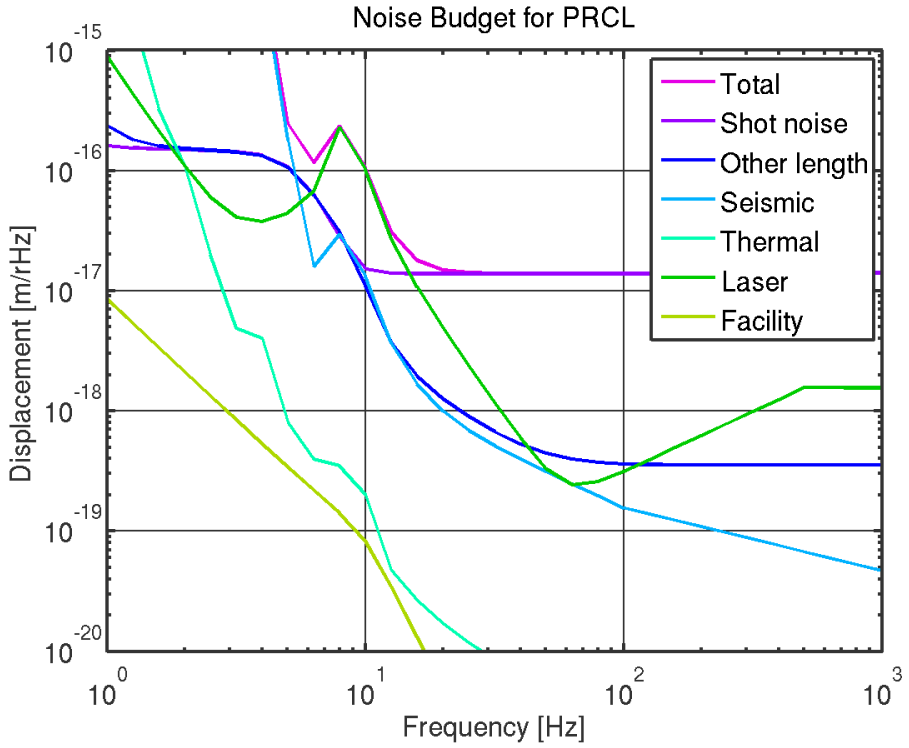

Figure 23: PRCL noise budget for No-SRM (no signal recycling mirror) operation. The Schnupp asymmetry is left at 5 cm and $f2 = 5 \times f1$ is used for MICH sensing.

Port	CARM	DARM	PRCL	MICH	SRCL	IMCL
REFL DC	1.1e+07	9.1e+04	2e+06	1e+06	4.6e+05	0.0055
REFL I1	**9.4e+08**	2e+05	7.3e+07	1.1e+06	**5.5e+03**	0.49
REFL Q1	6.2e+05	1.5e+03	1.9e+06	5.2e+04	8.6e+02	0.00032
REFL IM	1.4e+06	**2.5e+04**	**5.1e+06**	4.5e+05	**2.8e+05**	0.00074
REFL QM	4.9e+06	5.9e+04	3e+06	1e+06	8.5e+04	0.0025
REFL IP	1.4e+06	2.6e+04	5e+06	4.6e+05	2.8e+05	0.00075
REFL QP	4.9e+06	5.8e+04	3.1e+06	1e+06	8.5e+04	0.0026
REFL I2	5.7e+08	1.3e+05	1.6e+07	1.5e+06	2.5e+05	0.29
REFL Q2	6.1e+08	1.9e+05	5.3e+06	3e+06	4.7e+04	0.31
AS DC	1.3e+06	**4.2e+09**	2.8e+05	1.5e+07	7.6e+06	0.00066
AS I1	1.4e+05	1.2e+07	5.5e+04	4e+04	2.7e+04	7.4e-05
AS Q1	2.9e+04	6.8e+06	4.9e+03	5.9e+04	1.3e+04	1.5e-05
AS IM	3e+03	3.5e+03	2.1e+03	2.9e+03	3.7e+02	1.6e-06
AS QM	2.2e+03	7.6e+03	3.4e+03	4.5e+03	1.6e+02	1.1e-06
AS IP	2.9e+03	6.2e+03	5.3e+02	3.8e+03	1.1e+02	1.5e-06
AS QP	1e+03	5.6e+03	3.5e+03	1.3e+03	3.9e+02	5.3e-07
AS I2	2e+06	6.2e+07	5.3e+05	2.4e+05	1e+05	0.001
AS Q2	2.6e+06	7e+07	2.1e+05	2.2e+05	9.4e+04	0.0013
POX DC	2.7e+05	5.4e+07	1.7e+05	1.7e+05	4.4e+04	0.00014
POX I1	3.1e+07	2.5e+06	**1.2e+07**	5.8e+04	6.5e+03	0.016
POX Q1	3.6e+06	2.8e+05	2.4e+05	8.2e+03	1.3e+03	0.0019
POX IM	1.6e+05	2.2e+03	6.7e+04	2.6e+04	1.5e+04	8e-05
POX QM	1.9e+05	3.5e+03	1.3e+05	4e+04	2.3e+03	9.9e-05
POX IP	1.5e+05	2.5e+03	7e+04	2.6e+04	1.5e+04	8e-05
POX QP	1.7e+05	3.3e+03	9.1e+04	4.1e+04	2.3e+03	8.8e-05
POX I2	4.2e+06	8.2e+05	2.4e+06	1.5e+05	**4.6e+04**	0.0022
POX Q2	1.5e+07	1.2e+06	**2.1e+06**	**5.3e+05**	4.2e+04	0.0079
POY DC	9.1e+04	5.5e+07	4.1e+04	2.1e+05	4.1e+04	4.7e-05
POY I1	3.1e+07	2.6e+06	**1.2e+07**	4.7e+04	7.3e+03	0.016
POY Q1	3.6e+06	3e+05	2.5e+05	1.3e+04	1.3e+03	0.0019
POY IM	3.4e+04	8.7e+02	6.7e+04	1.3e+04	5.7e+03	1.8e-05
POY QM	1.6e+05	1.3e+03	8.5e+04	2.3e+04	3.3e+03	8.3e-05
POY IP	3.3e+04	5.6e+02	6.5e+04	1.3e+04	5.7e+03	1.7e-05
POY QP	1.5e+05	1.5e+03	7e+04	2.3e+04	3.3e+03	7.9e-05
POY I2	9.9e+06	6.4e+05	2.7e+06	1.5e+05	**1.1e+04**	0.0051
POY Q2	1.1e+07	8.2e+05	**6.5e+05**	**3.3e+05**	2.5e+04	0.0059
POB DC	3e+05	5.4e+07	1.8e+05	2.3e+05	4.4e+04	0.00015
POB I1	3.2e+07	3.7e+06	**1.2e+07**	4.9e+04	7.3e+03	0.016
POB Q1	3.7e+06	4.1e+05	2.5e+05	2e+04	3.4e+02	0.0019
POB IM	1.6e+05	2.4e+03	6.9e+04	2.7e+04	1.5e+04	8.5e-05
POB QM	1.9e+05	3.7e+03	1.4e+05	4.1e+04	2.3e+03	0.0001
POB IP	1.6e+05	2.7e+03	7.1e+04	2.6e+04	1.5e+04	8.4e-05
POB QP	1.7e+05	3.4e+03	9.4e+04	4.2e+04	2.3e+03	9e-05
POB I2	4.3e+06	8e+05	2.4e+06	1.6e+05	**4.6e+04**	0.0022
POB Q2	1.6e+07	1.8e+06	**2.2e+06**	**6e+05**	4.7e+04	0.0082
POP1 DC	1.7e+05	2e+04	1e+05	3e+04	4.6e+03	8.6e-05
POP1 I1	3.1e+07	6.5e+03	**1.2e+07**	6.1e+03	3e+02	0.016
POP1 Q1	3.6e+06	7.4e+02	2.4e+05	1.9e+03	12	0.0019
POP1 IM	1.1e+05	8.3e+02	3.4e+04	1.6e+04	9.4e+03	5.9e-05
POP1 QM	1.7e+05	1.9e+03	1.1e+05	3.3e+04	2.8e+03	8.6e-05
POP1 IP	1.1e+05	8.3e+02	3.5e+04	1.5e+04	9.4e+03	5.9e-05
POP1 QP	1.5e+05	1.9e+03	8.3e+04	3.3e+04	2.8e+03	7.9e-05
POP1 I2	5.7e+06	8.3e+02	2.6e+06	1.5e+05	**2.7e+04**	0.003
POP1 Q2	1.4e+07	2.3e+04	**1.4e+06**	**4.2e+05**	2.9e+04	0.0074
POP2 DC	1.7e+05	2.1e+04	1e+05	3.1e+04	4.9e+03	8.6e-05
POP2 I1	3.2e+07	6.7e+03	**1.2e+07**	**6.8e+03**	**3.1e+02**	0.017
POP2 Q1	3.7e+06	7.5e+02	2.5e+05	1.9e+03	12	0.0019
POP2 IM	1.2e+05	8.6e+02	3.7e+04	1.6e+04	9.8e+03	6.1e-05
POP2 QM	1.7e+05	1.9e+03	1.1e+05	3.5e+04	2.9e+03	8.9e-05
POP2 IP	1.2e+05	8.6e+02	3.9e+04	1.6e+04	9.8e+03	6.1e-05
POP2 QP	1.6e+05	1.9e+03	8.6e+04	3.5e+04	2.9e+03	8.2e-05
POP2 I2	6.2e+06	8.6e+02	2.6e+06	1.5e+05	2.8e+04	0.0032
POP2 Q2	1.5e+07	2.3e+04	**1.4e+06**	**4.3e+05**	**3e+04**	0.0076
OMC DC	4.4e+07	7.1e+05	2e+07	1.2e+07	7.3e+06	0.023
OMC I1	6.1e+03	1.2e+04	3.3e+03	3e+03	2.9e+02	3.1e-06
OMC Q1	5.4e+02	1.7e+05	6.9e+02	1.1e+03	4.1e+02	2.8e-07
OMC IM	1.1e+06	2.2e+04	1.8e+06	4.7e+05	2.2e+05	0.00057
OMC QM	1.7e+06	3.1e+04	1.3e+06	2.8e+06	3.3e+03	0.00088
OMC IP	1e+06	2e+04	1.8e+06	1.8e+05	2.2e+05	0.00052
OMC QP	1.3e+06	1.1e+04	6.3e+05	2.2e+06	5e+03	0.00068
OMC I2	1.7e+03	5.5e+06	1.9e+02	1.9e+04	3.2e+03	9.1e-07
OMC Q2	3.6e+02	1e+06	87	3.1e+03	5.8e+02	1.9e-07
TRX DC	7.8e+02	2.4e+06	1.8e+02	8.3e+03	1.9e+03	4e-07
TRY DC	6.8e+02	2.4e+06	1.6e+02	8.3e+03	1.9e+03	3.5e-07

Table 7: Sensing matrix at 1000 Hz, NSNS tuning, no closed loops, calculated by Optickle. Bold red shows the main elements used for control. Alternative error signals and important cross-couplings are marked with different collors. POP1 is the power recycling cavity pick off for light travelling from the PRM to the BS, while POP2 sees the light travelling from BS to PRM. The contractions used in the port name are: I: I-phase, Q: Q-phase, 1: demodulated at f_1, 2: demodulated at f_2, M: demodulated at $f_2 - f_1$, P: demodulated at $f_2 + f_1$. The units are Watts per meter.

Port	CARM	DARM	PRCL	MICH	SRCL	IMCL
REFL DC	1.7e+06	3e+04	5e+03	3.3e+04	5e+02	0.0009
REFL I1	**9.4e+08**	1.3e+05	7.3e+07	1e+06	**1.4e+04**	0.49
REFL Q1	7.4e+05	2.9e+03	2e+06	7.3e+04	3.1e+03	0.00038
REFL IM	1e+03	**2e+02**	**1e+03**	3.1e+02	92	5.4e-07
REFL QM	4.5e+03	6.2e+02	6.3e+02	7.7e+02	35	2.3e-06
REFL IP	2.7e+03	4.8e+02	1.1e+03	5.9e+02	89	1.4e-06
REFL QP	3.4e+03	4.5e+02	5.5e+02	6e+02	34	1.8e-06
REFL I2	4.3e+08	1.4e+05	8.6e+06	1.9e+06	1.9e+06	0.22
REFL Q2	3.6e+08	3e+05	9.9e+06	5.1e+06	2.8e+05	0.19
AS DC	3e+06	**9.7e+09**	6.7e+05	3.4e+07	7e+03	0.0016
AS I1	1.3e+05	3.3e+07	5.1e+04	1.3e+05	5.6e+03	6.8e-05
AS Q1	6.7e+04	1.7e+07	1.9e+04	5.3e+04	2.7e+03	3.5e-05
AS IM	2.1e+02	0.78	0.99	34	8.8	1.1e-07
AS QM	4.2e+02	1.1	1.3	18	19	2.2e-07
AS IP	3.6e+02	0.95	1.2	17	16	1.9e-07
AS QP	3.1e+02	0.97	1.1	19	14	1.6e-07
AS I2	5.8e+05	1.3e+08	1.3e+05	5e+05	9.7e+03	0.0003
AS Q2	7.5e+05	2e+08	5.8e+04	7.3e+05	2.7e+04	0.00039
POX DC	4.1e+04	7.2e+05	9e+03	4.8e+03	1.4e+05	2.1e-05
POX I1	3.1e+07	7.8e+06	**1.2e+07**	4.6e+04	1.2e+03	0.016
POX Q1	3.6e+06	8.7e+05	2.4e+05	1e+04	6.5e+02	0.0019
POX IM	1e+02	1.4	15	11	7.8	5.4e-08
POX QM	32	1.2	17	3.2	3.7	1.6e-08
POX IP	1.1e+02	1.5	16	11	8.1	5.8e-08
POX QP	28	1	7.8	3.1	3.4	1.4e-08
POX I2	6.1e+06	1.4e+06	1.7e+06	4.5e+04	**4.3e+05**	0.0032
POX Q2	1.2e+07	3.3e+06	**1.1e+06**	**9.5e+05**	2.2e+05	0.0064
POY DC	4.2e+04	7.5e+05	9.3e+03	3.6e+03	1.4e+05	2.2e-05
POY I1	3.1e+07	8e+06	**1.2e+07**	3.9e+04	1.6e+03	0.016
POY Q1	3.6e+06	9e+05	2.5e+05	1.5e+04	6.6e+02	0.0019
POY IM	95	1.3	5.1	2.7	4.6	4.9e-08
POY QM	20	0.42	14	0.61	1.1	1e-08
POY IP	95	1.3	7.7	2.6	4.8	4.9e-08
POY QP	19	0.52	9.2	1.2	0.76	9.7e-09
POY I2	1.1e+07	2.8e+06	1.7e+06	1.5e+05	**1.4e+05**	0.0056
POY Q2	5e+06	1.3e+06	**3.9e+05**	**4.9e+05**	1.2e+05	0.0026
POB DC	4.4e+04	9.2e+05	9.9e+03	3.6e+03	1.4e+05	2.3e-05
POB I1	3.2e+07	8.9e+06	**1.2e+07**	4.1e+04	1.7e+03	0.016
POB Q1	3.7e+06	9.9e+05	2.5e+05	1.8e+04	4.1e+02	0.0019
POB IM	1.2e+02	1.4	16	11	8.1	6.1e-08
POB QM	33	1.2	17	3.4	4.1	1.7e-08
POB IP	1.3e+02	1.5	17	11	8.4	6.5e-08
POB QP	29	1	7.7	3.4	3.7	1.5e-08
POB I2	6.3e+06	1.6e+06	1.8e+06	3.3e+04	**4.4e+05**	0.0032
POB Q2	1.3e+07	3.7e+06	**1.2e+06**	**9.9e+05**	2.2e+05	0.0067
POP1 DC	4.3e+02	4.7e+03	13	4.8e+03	59	2.2e-07
POP1 I1	3.1e+07	4.3e+03	**1.2e+07**	5.9e+03	2.9e+02	0.016
POP1 Q1	3.6e+06	5e+02	2.4e+05	2e+03	12	0.0019
POP1 IM	36	1.1	17	5	3.1	1.9e-08
POP1 QM	12	0.89	6.3	4	1.1	6.1e-09
POP1 IP	38	1.2	14	5	3.1	2e-08
POP1 QP	12	0.87	3.5	4	1.1	6.1e-09
POP1 I2	8.3e+06	8.8e+03	1.7e+06	9.7e+04	**2.9e+05**	0.0043
POP1 Q2	8.7e+06	4.1e+04	**4.5e+05**	**7.2e+05**	8.6e+04	0.0045
POP2 DC	4.3e+02	4.8e+03	15	4.9e+03	61	2.2e-07
POP2 I1	3.2e+07	4.4e+03	**1.2e+07**	**6.6e+03**	**3e+02**	0.017
POP2 Q1	3.7e+06	5.1e+02	2.5e+05	2e+03	11	0.0019
POP2 IM	37	1.2	18	5.4	3.3	1.9e-08
POP2 QM	14	0.75	6.3	4.5	1.1	7.2e-09
POP2 IP	39	1.2	15	5.4	3.3	2e-08
POP2 QP	14	0.76	3.5	4.4	1.1	7.1e-09
POP2 I2	8.7e+06	9e+03	1.8e+06	9.9e+04	**3e+05**	0.0045
POP2 Q2	8.7e+06	4.2e+04	**4.6e+05**	**7.4e+05**	**8.8e+04**	0.0045
OMC DC	3.9e+04	1e+03	9e+03	7.6e+03	2.8e+03	2e-05
OMC I1	8.5e+03	3.4e+05	2.5e+03	2.9e+03	1.7e+03	4.4e-06
OMC Q1	2.4e+03	2.8e+05	9.6e+02	1.1e+03	1.2e+03	1.3e-06
OMC IM	7.1e+02	18	2e+02	74	72	3.7e-07
OMC QM	4.7e+02	14	94	3e+02	37	2.4e-07
OMC IP	9.3e+02	25	1.5e+02	3.3e+02	75	4.8e-07
OMC QP	4e+02	11	1.1e+02	18	38	2.1e-07
OMC I2	4.6e+03	1.4e+07	8.6e+02	5e+04	2.3e+03	2.4e-06
OMC Q2	23	1.3e+04	56	5.1e+02	2.2	1.2e-08
TRX DC	69	4e+03	18	32	6e+03	3.6e-08
TRY DC	98	4e+03	18	36	6e+03	5.1e-08

Table 8: Sensing matrix at 1000 Hz, zero detuning, no closed loops, calculated by Optickle. Bold red shows the main elements used for control. Alternative error signals and important cross-couplings are marked with different collors. POP1 is the power recycling cavity pick off for light travelling from the PRM to the BS, while POP2 sees the light travelling from BS to PRM. The contractions used in the port name are: I: I-phase, Q: Q-phase, 1: demodulated at f_1, 2: demodulated at f_2, M: demodulated at $f_2 - f_1$, P: demodulated at $f_2 + f_1$. The units are Watts per meter.

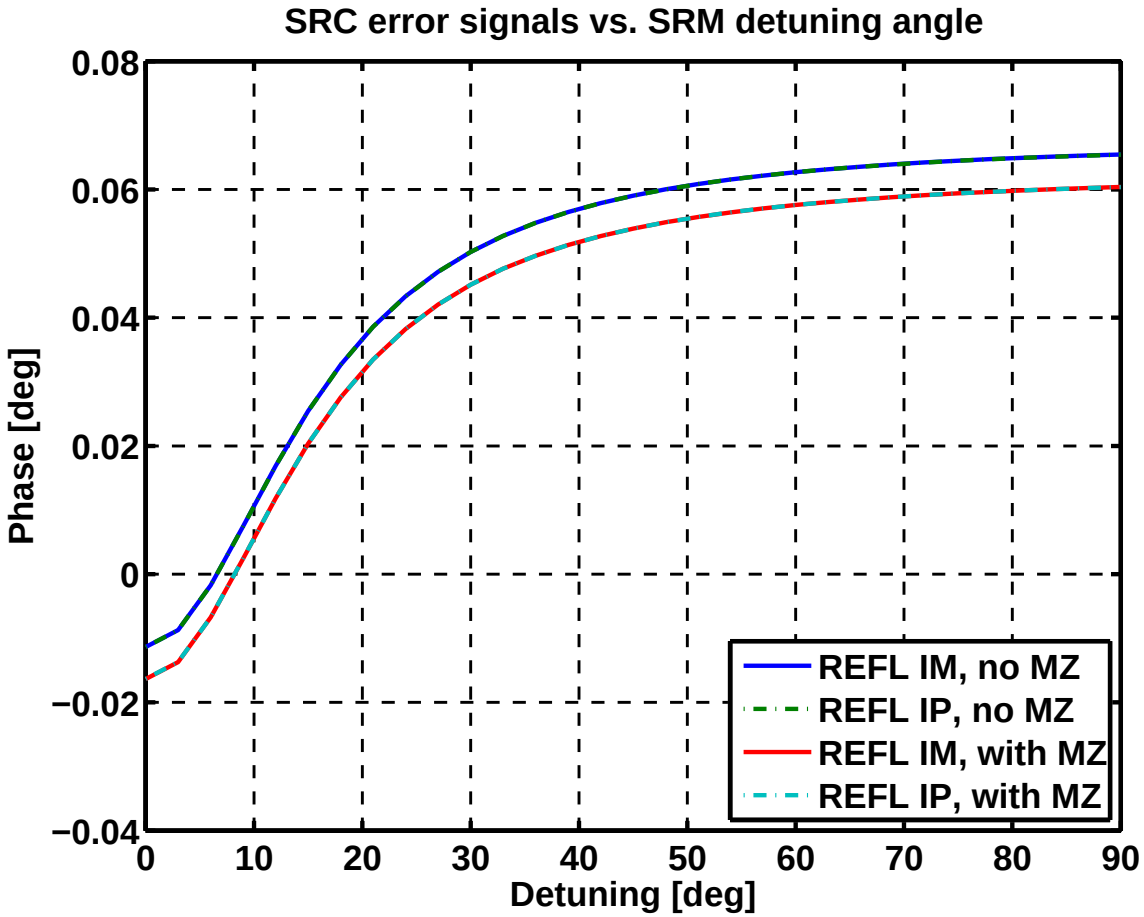

Figure 24: REFL double demodulation error signals with and without a Mach-Zehnder Interferometer. The difference is due to direct beating of 4xf1 and 6xf1 sidebands against the carrier, and hence is proportional to amount of carrier reflected from the interferometer.

Port	CARM	DARM	PRCL	MICH	SRCL	IMCL
REFL I1	**2.8e+09**	7.7e+07	1.5e+08	3e+06	**2e+05**	1.5
AS DC	1.4e+06	**3.8e+09**	2.7e+05	1.3e+07	1.1e+07	0.0007
POX I1	3.2e+07	2.1e+06	**1.3e+07**	**1.1e+04**	**6.6e+03**	0.016
POX Q2	4.6e+06	4.4e+05	**1.5e+06**	**1.3e+06**	**1.1e+04**	0.0024
REFL IM	2.3e+05	**3e+05**	**2.7e+07**	4.1e+05	**2.1e+06**	0.00012
REFL I2	5.1e+08	1.4e+07	4.3e+07	2.9e+05	9.2e+05	0.26
POX I2	1.9e+07	1.2e+06	3.8e+06	9.4e+02	8.5e+04	0.0099
IMC I3	7.3e+09	0	0	0	0	**0.0083**

Table 9: Sensing matrix at 20 Hz with Mach-Zehnder, NSNS tuning

Port	CARM	DARM	PRCL	MICH	SRCL	IMCL
REFL I1	**2.8e+09**	7.7e+07	1.5e+08	3e+06	**1.4e+05**	1.5
AS DC	1.4e+06	**3.8e+09**	2.7e+05	1.3e+07	1.2e+07	0.0007
POX I1	3.2e+07	2.1e+06	**1.4e+07**	**1.1e+04**	**6.6e+03**	0.016
POX Q2	4.6e+06	4.5e+05	**1.5e+06**	**1.3e+06**	**1.1e+04**	0.0024
REFL IM	2.4e+05	**3.3e+05**	**2.7e+07**	4.2e+05	**2.1e+06**	0.00013
REFL I2	5.1e+08	1.5e+07	5.5e+07	3.7e+05	9.2e+05	0.26
POX I2	1.9e+07	1.2e+06	3.8e+06	9.5e+02	8.5e+04	0.0099
IMC I3	7.4e+09	0	0	0	0	**0.0083**

Table 10: Sensing matrix at 20 Hz no Mach-Zehnder, NSNS tuning

Port	CARM	DARM	PRCL	MICH	SRCL	IMCL
REFL I1	**2.8e+09**	5.9e+05	1.5e+08	3.3e+06	**4.1e+03**	1.4
AS DC	1.2e+06	**4.2e+09**	3e+05	1.5e+07	7.7e+06	0.00064
POX I1	3.1e+07	2.5e+06	**1.3e+07**	**1.9e+04**	**6.6e+03**	0.016
POX Q2	4.5e+06	6.1e+05	**1.5e+06**	**1.3e+06**	**1.1e+04**	0.0024
REFL IM	1.1e+07	**1.9e+03**	**2.6e+07**	4e+05	**2.1e+06**	0.0059
REFL I2	5e+08	1.4e+05	4.4e+07	3.2e+05	9.4e+05	0.26
POX I2	1.9e+07	9.8e+05	3.8e+06	4e+04	8.4e+04	0.0098
IMC I3	7.3e+09	0	0	0	0	**0.41**

Table 11: Sensing matrix at 1000 Hz with Mach-Zehnder, NSNS tuning

Port	CARM	DARM	PRCL	MICH	SRCL	IMCL
REFL I1	**2.8e+09**	5.9e+05	1.5e+08	3.3e+06	**6.5e+04**	1.4
AS DC	1.3e+06	**4.3e+09**	3e+05	1.5e+07	7.8e+06	0.00065
POX I1	3.1e+07	2.6e+06	**1.3e+07**	**1.9e+04**	**6.6e+03**	0.016
POX Q2	4.6e+06	6.1e+05	**1.5e+06**	**1.3e+06**	**1.1e+04**	0.0024
REFL IM	1.2e+07	**9.7e+03**	**2.6e+07**	4.1e+05	**2.1e+06**	0.006
REFL I2	5e+08	1.4e+05	5.6e+07	4e+05	9.4e+05	0.26
POX I2	1.9e+07	9.9e+05	3.8e+06	4e+04	8.5e+04	0.0099
IMC I3	7.3e+09	0	0	0	0	**0.41**

Table 12: Sensing matrix at 1000 Hz no Mach-Zehnder, NSNS tuning

Port	CARM	DARM	PRCL	MICH	SRCL	IMCL
REFL I1	**2.8e+09**	2.6e+08	1.5e+08	4.2e+06	**8.2e+05**	1.5
AS DC	5.8e+06	**1.6e+10**	1.4e+06	5.7e+07	4.9e+07	0.003
POX I1	3.2e+07	1e+07	**1.3e+07**	**3.1e+04**	**3e+04**	0.016
POX Q2	4.2e+06	1.3e+06	**7.3e+05**	**9.4e+05**	**1.6e+05**	0.0022
REFL IM	2.5	**27**	**2.5e+02**	7.6	6.7	2.2e-09
REFL I2	7.3e+08	6.8e+07	2.8e+07	1.5e+06	4.6e+06	0.38
POX I2	1.3e+07	4.1e+06	2.2e+06	3.5e+02	**3.9e+05**	0.0068
IMC I3	7.3e+09	0	0	0	0	**0.0083**

Table 13: Sensing matrix at 20 Hz with Mach-Zehnder, zero detuning

Port	CARM	DARM	PRCL	MICH	SRCL	IMCL
REFL I1	**2.8e+09**	2.6e+08	1.5e+08	4.2e+06	**1.2e+06**	1.5
AS DC	5.8e+06	**1.6e+10**	1.4e+06	5.7e+07	5e+07	0.003
POX I1	3.2e+07	1e+07	**1.4e+07**	**3.2e+04**	**3e+04**	0.016
POX Q2	4.2e+06	1.3e+06	**7.4e+05**	**9.5e+05**	**1.6e+05**	0.0022
REFL IM	1.4e+04	**1.3e+05**	**1.1e+02**	2e+03	4.2e+02	7.1e-06
REFL I2	7.4e+08	6.9e+07	4e+07	1.6e+06	4.6e+06	0.38
POX I2	1.3e+07	4.1e+06	2.2e+06	3.6e+02	**3.9e+05**	0.0068
IMC I3	7.4e+09	0	0	0	0	**0.0083**

Table 14: Sensing matrix at 20 Hz no Mach-Zehnder, zero detuning

C Appendix: Bench, Optickle and Looptickle simulation code and configuration files

Much of the LSC optimization was done with Bench62, Optickle and Looptickle. These software packages are available in CVS at emvogil-3.mit.edu:/export/cvs/iscmodeling

- Bench62
- Optickle
- Looptickle

Port	CARM	DARM	PRCL	MICH	SRCL	IMCL
REFL I1	**2.8e+09**	4e+05	1.5e+08	3.3e+06	**4.2e+03**	1.4
AS DC	2.9e+06	**9.8e+09**	6.8e+05	3.5e+07	7.2e+03	0.0015
POX I1	3.1e+07	7.8e+06	**1.3e+07**	**3.3e+04**	**1.2e+03**	0.016
POX Q2	4.1e+06	1e+06	**7.1e+05**	**9.4e+05**	**1.6e+05**	0.0021
REFL IM	1.2e+02	**0.41**	**2.5e+02**	6.3	6.7	6.5e-08
REFL I2	7.3e+08	1.1e+05	2.7e+07	1.2e+06	4.8e+06	0.38
POX I2	1.3e+07	3.2e+06	2.2e+06	1.8e+04	**4e+05**	0.0067
IMC I3	7.3e+09	0	0	0	0	**0.41**

Table 15: Sensing matrix at 1000 Hz with Mach-Zehnder, zero detuning

Port	CARM	DARM	PRCL	MICH	SRCL	IMCL
REFL I1	**2.8e+09**	4e+05	1.5e+08	3.3e+06	**3.6e+05**	1.5
AS DC	2.9e+06	**9.9e+09**	6.9e+05	3.5e+07	7.3e+03	0.0015
POX I1	3.1e+07	7.9e+06	**1.3e+07**	**3.4e+04**	**1.2e+03**	0.016
POX Q2	4.1e+06	1e+06	**7.2e+05**	**9.5e+05**	**1.6e+05**	0.0021
REFL IM	1.3e+04	**1.9e+03**	**1.4e+02**	1.9e+03	23	6.9e-06
REFL I2	7.4e+08	1.1e+05	3.9e+07	1.3e+06	4.8e+06	0.38
POX I2	1.3e+07	3.3e+06	2.2e+06	1.9e+04	**4e+05**	0.0068
IMC I3	7.3e+09	0	0	0	0	**0.41**

Table 16: Sensing matrix at 1000 Hz no Mach-Zehnder, zero detuning

Time domain simulations for lock acquisition have been developed using the LIGO time domain model E2E (http://www.ligo.caltech.edu/ e2e/).

References

[1] L. Barsotti, *Lock acquisition study for Advanced LIGO*, LIGO-T1000294.

[2] P. Fritschel, *Advanced LIGO Systems Design*, LIGO-T010075-v2.

[3] S. Ballmer, "LIGO Interferometer Operating as a Radiometer", `http://www.ligo.caltech.edu/docs/P/P060043-00.pdf`

[4] H. Grote, *High power, low-noise, and multiply resonant photodetector for interferometric gravitational wave detectors*, Rev. Sci. Instrum. **78,** 054704 (2007). LIGO-P-060032-00-Z.

[5] R. Abbott, *RFPD Topology Comparison*, LIGO-T060268-02-C.

[6] B. Lantz, *Development of Improved Photodiodes for Advanced LIGO*, LIGO-T070018-00-R.

[7] K. Kawabe, *Orientation of Quadrant Diode for Wave Front Sensing*, LIGO-T060035-0-D.

[8] P. Fritschel, *Backscattering from the AS port: Enhanced and Advanced LIGO*, LIGO-T060303-00-D.

[9] V. Mandic, *Estimate of the Beam Jitter at the Output Mode Cleaner*, LIGO-T060178-00-D.

[10] SPI feasibility study, to be distributed by ANU.

[11] Osamu Miyakawa et al. *J. Phys.: Conf. Ser.* **32** 265-269 (2006)

[12] K Arai et al. *Class. Quantum Grav.* **19** 1843-184 (2002)

[13] Miyakawa and Yamamoto *Lock Acquisition Studies for Advanced Interferometers*, Proceedings Amaldi 2007

[14] M.Evans et al. *Lock acquisition of a gravitational-wave interferometer*, Optics Letters vol.27, n.8, April 15 (2002)